ELSEVIER

Biochimica et Biophysica Acta 1462 (1999) 109–140

BIOCHIMICA ET BIOPHYSICA ACTA
BBA

www.elsevier.com/locate/bba

Review

The monolayer technique: a potent tool for studying the interfacial properties of antimicrobial and membrane-lytic peptides and their interactions with lipid membranes

Régine Maget-Dana *

Centre de Biophysique Moléculaire, rue Charles Sadron, 45071 Orléans cedex 2, France

Accepted 5 October 1999

Abstract

Erudites of the antiquity already knew the calming effect of oil films on the sea waves. But one had to wait until 1774 to read the first scientific report on oil films from B. Franklin and again 1878 to learn the thermodynamic analysis on adsorption developed by J. Gibbs. Then, in 1891, Agnes Pockels described a technique to manipulate oil films by using barriers. Finally, in 1917, I. Langmuir introduced the experimental and theoretical modern concepts on insoluble monolayers. Since that time, and because it has been found to provide invaluable information at the molecular scale, the monolayer technique has been more and more extensively used, and, during the past decade, an explosive increase in the number of publications has occurred. Over the same period, considerable and ever-increasing interest in the antimicrobial peptides of various plants, bacteria, insects, amphibians and mammals has grown. Because many of these antimicrobial peptides act at the cell membrane level, the monolayer technique is entirely suitable for studying their physicochemical and biological properties. This review describes monolayer experiments performed with some of these antimicrobial peptides, especially gramicidin A, melittin, cardiotoxins and defensin A. After giving a few basic notions of surface chemistry, the surface-active properties of these peptides and their behavior when they are arranged in monomolecular films are reported and discussed in relation to their tridimensional structure and their amphipathic character. The penetration of these antimicrobial peptides into phospholipid monolayer model membranes, as well as their interactions with lipids in mixed films, are also emphasized.

Keywords: Antimicrobial peptide; Membrane-lytic peptide; Surface-active property; Lipid monolayer; Lipid–peptide interaction; Monolayer technique

Abbreviations: BLM, bilayer lipid membrane; CTX, cardiotoxin; CTX RM, cardiotoxin reduced and methylated; DLPS, dilauroylphosphatidylserine; DMPC, dimyristoylphosphatidylcholine; DMPA, dimyristoylphosphatidic acid; DMPG, dimyristoylphosphatidylglycerol; DOPC, dioleoylphosphatidylcholine; DOPE, dioleoylphosphatidylethanolamine; DOPG, dioleoylphosphatidylglycerol; DPPA, dipalmitoylphosphatidic acid; DPPC, dipalmitoylphosphatidylcholine; DPPE, dipalmitoylphosphatidylethanolamine; DPPG, dipalmitoylphosphatidylglycerol; egg-PC, phosphatidylcholine extracted from egg yolk; FTIR, Fourier-transformed infra red spectroscopy; GA, gramicidin A; HNP, human neutrophil peptide; IRRAS, infrared external reflection-absorption spectroscopy; L-C, liquid-condensed state; L-E, liquid-expanded state; LUV, large unilamellar vesicles; PS, phosphatidylserine; QCM, quartz-crystal microbalance; SUV, single unilamellar vesicles

* Fax: +33-2-3863-1517; E-mail: maget@cnrs-orleans.fr

0005-2736/99/$ – see front matter
PII: S0005-2736(99)00203-5

Contents

1. Introduction

In the last decade, several reviews have been devoted to antimicrobial peptides [1–18] isolated from a wide variety of bacteria [9,19,20], plants [14], insects [3,5], amphibians [1] and mammals including humans [11], that is indicative of a growing interest in these compounds.

Table 1 lists some representative antimicrobial peptides of various origins. The upper part of Table 1 is devoted to host defense (also called immunogenic) peptides either induced in the insect hemolymph after septic injury, such as defensin A, or produced constitutively, such as frog skin magainins, androctonin or mammalian defensins. The second part of Table 1 concerns peptides generally known as toxins

Table 1
Main characteristics of some antimicrobial peptides [21–33].

Peptide	Primary sequence	(a)	(b)	(c)	(d)	Origin	References
Androctonin	**R**SVC**R** QIK**I**C **RR**RGG CYY**K**C TN**R**PY	+8	1.08	2	β-hairpin	*Androctonus australis* (scorpion hemolymph)	[21]
Defensin A	ATC**D**L LSGTG INHSA CAAHC LL**R**GN **R**GGYC NG**K**GV CVC**R**N	+3	0.6	3	CSαβ	*Phormia terranovae* (fleshfly larvae hemolymph)	[22, 23]
Magainin 1	GIG**K**F LHSAG **K**FGK**A** FVGE**I** M**K**S	+3	0.53	0	α-helix	*Xenopus laevis* (frog skin)	[24]
Rat Defensin (RatNP -2)	VTCYC **R**STR**C** GF**RER** LSGAC GY**R**G**R** IYRLC **CR**	+7	0.68	3	β-sheet	rat neutrophils	[25]
Melittin	GIGAV L**K**VLT TGLPA LISWI **KRK**RQ Q	+5	0.86	0	α-helix	*Apis mellifera* (honey bee venom)	[26]
Bombolitin III	I**K**IM**D** ILA**K**L G**K**VLA HV	+2	0.54	0	α-helix	*Megabombus pennsylvanicus* (bumblebee venum)	[27]
Cardiotoxin I	L**K**CNQ LIPPF W**K**TCP **K**GK**N**L CY**K**MT M**R**AAP MVPV**K** **R**GC**I**D VCP**K**S SLLI**K** YMCCN TN**K**CN	+10	0.93	4	β-sheet	*Naja mo. mossambica* (cobra venom)	[28]
Nisin Z	IOAIU LAA*PG AKA*GA LMGAN MKA*AA* AHASI HVU**K**	+3	0.31	5	β-turns	*Lactococcus lactis*	[29, 30]
δ Lysin	f MAQD**I** ISTIG **D**LV**K**W I**I**DTV N**K**FT**K** **K**	+1	0.86	0	α-helix	*Staphylococcus aureus*	[31]
Gramicidin A	f XGALA VVVWL WLWLW Et	0	0.07	0	α-helix	*Bacillus brevis*	[32, 33]

A A=lanthionine; A A*=3 methyllanthionine; Et=ethanolamine; f=formyl; O=dehydrobutyrine; U=dehydroalanine; X=V or I; └S┘ └S┘.
CSαβ= cysteine stabilized αβ motif; bold letters: charged residues; (a) net charge at pH 7; (b) Polar/nonpolar amino acid ratio; (c) number of disulfide bonds; (d) Predominant secondary structure.

and characterized by a high lytic activity. All these compounds possess the following features in common: (1) they have a small molecular weight (less than 7000 kDa); (2) they are cationic; (3) they are amphiphilic, as attested by the value of the polar/non-polar amino acid ratio which, apart for nisin Z, varies from 0.5 to 1.2; and (4) they have the capacity to adopt a secondary structure: linear peptides, such as magainins, melittin or δ-lysin, adopt an amphiphilic α-helical conformation; the others, such as defensins, cardiotoxins or nisins possess several disulfide bridges (or lanthionine bonds) that stabilize a rigid structure. Finally, at the bottom of Table 1 we find gramicidin A, a bacterial antibiotic better known as an ionophoric agent, which is a highly hydrophobic compound devoid of charged residues, unlike the above-mentioned peptides.

These antimicrobial peptides are known to act at the membrane level of the sensitive cells and their biological activity appears to be directly related to their sequence and structural characteristics. Their amphipathy allows them to be both soluble in an aqueous medium such as the extracellular medium and to diffuse towards polar/apolar interfaces such as the extracellular medium/cell membrane interface. Another consequence of their amphipathy is their natural tendency to self-associate. Melittin, although very soluble in water (up to 250 mg/ml [2]) undergoes a monomeric/tetrameric transition depending on ionic, pH and concentration conditions [34]. Magainins are monomeric up to 10 mM because they are structureless below this concentration [35], but they polymerize in filaments at higher concentrations [36]. Similarly δ-lysin [37,38] and bombolitin III [39] precipitate in large aggregates. Human α-defensins exist as dimers [10] and the insect defensin A was also found to be self-associated in aqueous solutions [40].

Being highly cationic, antimicrobial peptides inter-

act preferentially with acidic lipids which are particularly abundant in bacterial membranes [41]. It has therefore been suggested that differences in the amount of acidic membrane phospholipids play a major role in sensitive cell specificity [42]. In particular, antimicrobial peptides bind to lipopolysaccharides on the outer membrane of Gram-negative bacteria, leading to the disruption of this first barrier [43]. However, the killing event for both Gram-negative and Gram-positive bacteria is the permeabilization of the cytoplasmic membrane induced by the formation of voltage-dependent channels, as demonstrated with numerous peptides such as mammalian defensins [44], insect defensins [45], magainins [46], melittin [47] and nisins [48]. In the case of linear peptides, channels within the cytoplasmic membrane are thought to be made of bundles of α-helices [13] whereas, for β-sheet peptides, dimer associations may be the basis of the channel structures [49]. The hydrophobic gramicidin A forms helical dimer channels specific for the transport of monovalent cations across membranes [50–52].

The amphipathic character of antimicrobial peptides makes them surface-active products and as their biological activity occurs at lipid membrane interfaces, the monolayer technique is entirely suitable to study their physicochemical and biological properties.

In this review, we will describe some aspects of this technology by focusing on the procedures needed to investigate a particular property or phenomenon, such as adsorption of amphipathic peptides at the air/water interface, their behavior when arranged in a monomolecular film, how they penetrate into a phospholipid monolayer taken as a membrane model and finally their interactions with lipid molecules in a mixed peptide–lipid monolayer. Each procedure will be illustrated with examples of investigations performed on some antimicrobial peptides.

2. Elementary notions of surface chemistry

In the following, all the basic notions concerning surface chemistry are based on the book by Adamson [53] and by that of Gaines [54], still considered as the bible for research workers in the field of monomolecular films.

2.1. Interfaces

'Interfaces' refers to the boundary regions between two phases in equilibrium, liquid–liquid, liquid–gaseous, liquid–solid or solid–solid phases. Our purpose will be restricted here to liquid–gaseous interfaces. At an interface, there is a transition between the composition and properties of the two bulk phases which it separates. This transition is not more than one or two molecules deep in thickness [55] and constitutes the interfacial region. To analyze the situation within the interfacial region, Gibbs [56] introduced an imaginary mathematical dividing surface (Fig. 1a), and in this reference system it is assumed that all the extensive properties (energy, entropy, composition, etc.) are unchanged up to the dividing surface. Thus, in the real system, there will be an *excess quantity* (positive or negative) of these various properties as compared with the reference system.

2.2. Surface tension

The mathematical treatment given by Gibbs [56] indicates that for any variation from equilibrium at a plane and fluid interface:

$$\mathrm{d}U = T\mathrm{d}S + \sum \mu_i \, \mathrm{d}n_i - P\mathrm{d}V + \gamma \, \mathrm{d}s \qquad (1)$$

where U is the internal energy of the system, S is the entropy, μ_i and n_i are the chemical potential and the mole number of component i, respectively, s is the total interfacial area and γ is the *surface tension* of the interface.

Since the Gibbs free energy $G = U - TS + PV$, it follows that, at constant P and using the surface excess quantities:

$$\mathrm{d}G^{\mathrm{ex}} = -S^{\mathrm{ex}}\mathrm{d}T + \sum \mu_i \, \mathrm{d}n_i^{\mathrm{ex}} + \gamma \, \mathrm{d}s \qquad (2)$$

and

$$\gamma = |\mathrm{d}G^{\mathrm{ex}}/\mathrm{d}s|_{T,P,n_i} \qquad (3)$$

In the case of a pure liquid in equilibrium with its saturated vapor, the surface tension is also equal to the surface excess of the Helmoltz free energy ($F = G - PV$) per unit area:

$$\gamma_0 = F_0^{\mathrm{ex}}/s$$

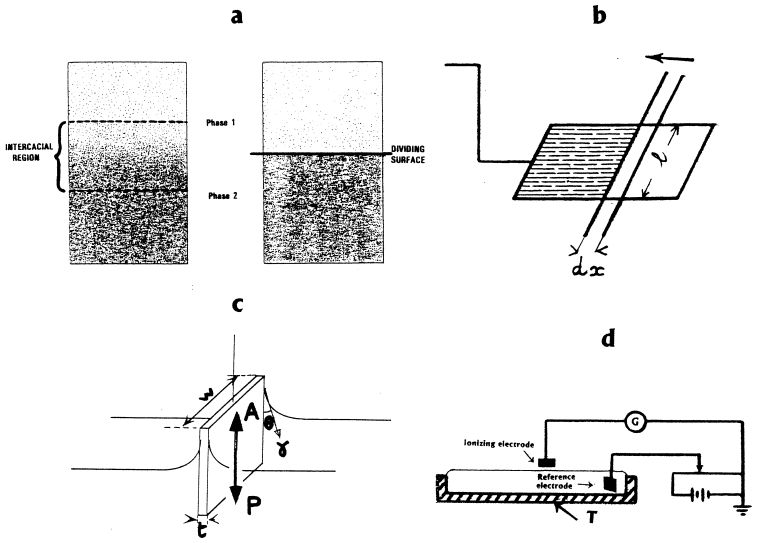

Fig. 1. Notions of surface chemistry. (a) Interface: actual system with an interfacial region between two phases (left) and reference system with the imaginary dividing surface according to Gibbs theory (from [54]). (b) Surface tension: the movable rod is put on the frame. When the film is broken on the right side of the frame, the rod covers the distance dx in the direction of the arrow, under the action of surface tension. (c) Wilhelmy plate: P is the weight of the thin plate, A is the Archimedes buoyancy, γ is the surface tension and θ is the contact angle of the plate with the liquid surface. (d) Ionizing electrode method for measuring surface potentials. G, galvanometer; T, trough in which interfacial experiments are performed; the reference electrode is immersed in the subphase.

To illustrate (Fig. 1b) the notion of surface tension, let us consider a wire frame dipped in a soap solution and then removed: a soap film is stretched over the frame. Then place a light rod across the frame and break the film on one side of the rod: the rod moves towards the film side under the action of a capillary force, tangent to the film surface, perpendicular to the movable rod and proportional to the length, l, of the rod. Then the work done in extending the movable rod a distance dx is:

$$\text{work} = \gamma\, l\, \mathrm{d}x$$

The surface tension is then a force per length unit, expressed as N/m. As an example, the surface tension of pure water, $\gamma_0 = 72.75$ mN/m [57].

2.3. Adsorption

The properties of an interface will be affected by changes in either of the two phases involved and especially by the presence of solutes in the liquid phase. Lipids, polymers, proteins... are called *biosurfactants* because, like soaps, they are interfacially active materials, i.e. substances able to adsorb at interfaces. These amphipathic compounds are asymmetrical molecules which have a great tendency to be oriented at the interface so as to provide the most gradual possible transition from one phase to the other. A molecule will be adsorbed from solution at an interface if the energy exchange with the surface overcomes the increase in free energy which accompanies the removal of the molecule from the solution.

By integration and total differentiation of Eq. 1 we obtain, at constant P, the surface analog of the Gibbs–Duhem equation in bulk:

$$S^{\mathrm{ex}}\mathrm{d}T + \sum n_i^{\mathrm{ex}}\mathrm{d}\mu_i + s\mathrm{d}\gamma = 0 \qquad (4)$$

At constant temperature and defining the *surface concentration* of component i,

$$\Gamma_i = n_i^{\mathrm{ex}}/s$$

$$\sum \Gamma_i \mathrm{d}\mu_i + \mathrm{d}\gamma = 0$$

For a two-component system (solvent:component 1+solute:component 2),

$$\mathrm{d}\gamma + \Gamma_1 \mathrm{d}\mu_1 + \Gamma_2 \mathrm{d}\mu_2 = 0$$

It is always possible to place the dividing surface

in such a position that the surface excess of solvent vanishes ($\Gamma_1 = 0$), then,

$$d\gamma = -\Gamma_2 d\mu_2$$

with $\mu_2 = \mu_2^0 + RT \ln a_2$ (a_2 being the activity of the solute and μ_2^0 the standard chemical potential of the solute)

$$\Gamma_2 = -1/RT \ (d\gamma/d\ln a_2)$$

If the solution is dilute enough so that the behavior is ideal, then the volume concentration, C, of the solute is proportional to the activity, and:

$$\Gamma = -1/RT \ (d\gamma/d\ln C) \quad (5)$$

This is the Gibbs adsorption isotherm widely used in evaluating the extent of adsorption of surface-active compounds in dilute solutions, from surface tension measurements. This relation shows clearly that if there is adsorption (that is to say a positive excess) of the solute at the interface, the surface tension of the solution decreases. The difference,

$$\pi = \gamma_{\text{solvent}} - \gamma_{\text{solution}}$$

is called *surface pressure* of the film formed by the adsorbed molecules.

2.4. Surface pressure measurements

A fluid interface, such as air/water interface, has the advantage of being a plane interface, the change in interfacial free energy of which can be obtained by a simple measurement of surface pressure.

Herein, we will describe only the Wilhelmy method which is the most commonly used to measure surface pressure of plane and fluid interfaces. A thin plate, usually made of glass, mica or platinum, is partially immersed in the liquid phase and is connected to an electromicrobalance. The forces acting on the plate are its weight P and surface tension effects downward, and Archimedes buoyancy A upward (Fig. 1c). The net downward force is:

$$F = P + 2\gamma(w + t)\cos\theta - A$$

where w and t ($t \ll w$) are the width and the thickness of the plate, respectively, and θ is the contact angle of the liquid with the solid plate. If the plate is completely wetted (platinum offers the advantage that flaming not only removes contaminants but also renders the plate wettable) the contact angle $\theta = 0$ and $\cos\theta = 1$, so that,

$$F = P + 2\gamma w - A$$

When the composition of the interface varies, P and A (provided the plate is maintained in a fixed position) stay constant, then,

$$\Delta F = 2w(\gamma_{\text{solution}} - \gamma_{\text{water}}) = -2w\pi$$

and

$$\pi = -\Delta F/2w$$

2.5. Surface potential

As seen above, there is a tendency for molecules near the liquid surface to have a specific orientation. The orientation of water molecules, which behave as dipoles, produces an asymmetrical field near the surface. Spreading a monolayer on a clean water surface, will produce a change in the orientation at the interface and then a change in the nature of the electrical field. The difference, ΔV, in surface potentials between that for the aqueous phase and that for the film covered phase, is attributed to the film. ΔV is called *surface potential* or 'Volta potential' and is also defined as the work required to bring a unit charge from infinity just up to the phase. A qualitative interpretation of ΔV is generally given in terms of analogy with a condenser: a polarized molecule with an effective *dipole moment*[1] $\mathcal{M} = qd$ is similar to two conducting plates separated by a distance d and enclosing a charge density q. Then, the potential difference ΔV is given by

$$\Delta V = 4\pi qd/\varepsilon$$

where ε is the dielectric constant.

If there is an array of n dipoles by area unit,

$$\Delta V = 4\pi n \, \mathcal{M}_\perp/\varepsilon$$

where $\mathcal{M}_\perp$ is the normal component of the dipole moment to the surface.

There are several contributions to ΔV: (1) the

[1] The dipole moment is expressed as Debye (D). As an example, the dipole moment of the peptide unit in an α-helix is 3.6 D [58].

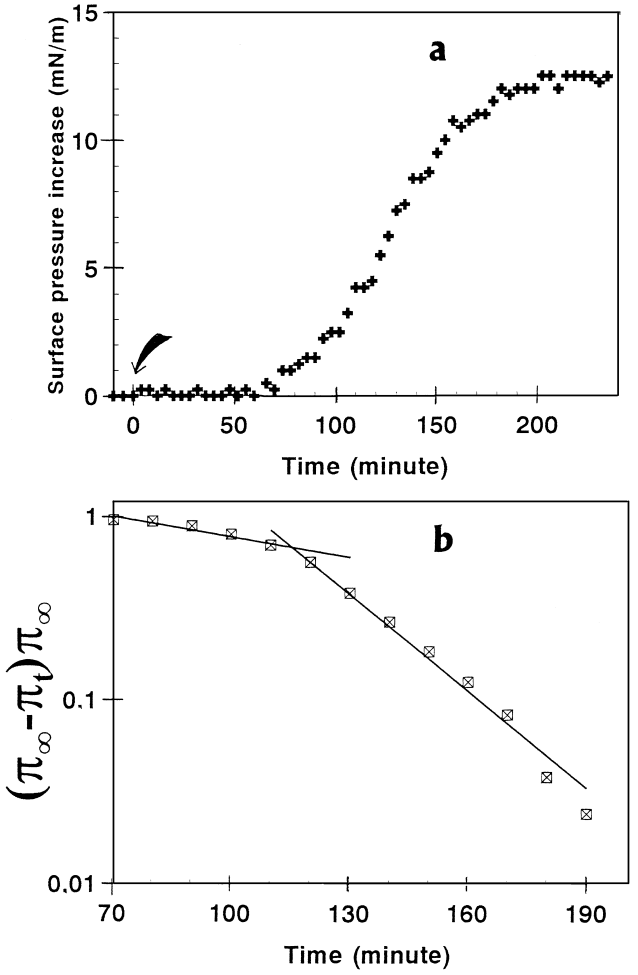

Fig. 2. Adsorption of peptides at the air/water interface. (a) Time dependence of defensin A adsorption ($\Delta\pi^{AW}$ versus t) plot. The defensin A concentration is 4×10^{-6} M(res) in 30 mM Tris-Cl, pH 7.4; $T=20$°C. Defensin A was added at the arrow. (b) Corresponding kinetics plot according to Eq. 8 [66].

change induced by the reorientation of the water dipoles in the presence of the film forming molecules; (2) the dipoles of the film forming molecules, namely that of the polar group and that of the alkyl part, which can be located in different dielectric constant media [59]; then,

$$\Delta V = 4\pi \sum (n\,\mathcal{M}_\perp/\varepsilon)$$

(3) we have seen that most of the antimicrobial peptides are positively charged molecules. Therefore there is an additional contribution to ΔV due to the Gouy–Chapman electrical double layer, arising from the charged monolayer and the counter-ions in the subphase solution.

The surface potential at a liquid interface is then given by:

$$\Delta V = 4\pi \sum (n\,\mathcal{M}_\perp/\varepsilon) + \Psi_0 \quad (6)$$

where the first term is the conventional surface dipole moment expression for uncharged monolayers and Ψ_0 represents the potential difference (due to the double layer) between the surface and the bulk of the subphase solution. The subscript 0 means that Ψ_0 is the potential at the distance $x=0$ from the interface.

The relevant principles of membrane electrochemistry are well described in [60].

2.6. Surface potential measurements

Surface potential measurements can be accomplished either by the ionizing electrode method or by the vibrating plate method. The first method involves ionization of the air above the film, so that it becomes conducting. The potential difference between two electrodes, one in the aqueous subphase and the other in the air above the surface, can then be measured directly. The ionization in the air above the film is produced by coating the air electrode with an α-emitter, such as polonium or americium. The reference electrode placed in the bulk subphase can be an Ag–AgCl electrode. The gap between the radioactive electrode and the liquid surface ($\sim$5 mm) is generally sufficiently conducting that ΔV can be measured by means of a high impedance (10^{16} Ω) voltameter. The principle of this method is shown in Fig. 1d.

In the vibrating plate method, the radioactive electrode is replaced by a vibrating electrode which constitutes one of the plates of a condenser, the second being the surface of the aqueous subphase. The alternating signal, generated across a resistance when the plate is vibrated rapidly, is detected using a high-gain amplifier.

3. Adsorption of antimicrobial peptides at the air/water interface

The adsorption of peptides at the air/water interface is therefore currently monitored by following the

increase in surface pressure as a function of time, as exemplified in Fig. 2a in the case of defensin A. The rate of adsorption is regulated by the rate of diffusion of the peptide molecules from the bulk solution, at a peptide concentration C, up to the subsurface close to the interface at zero peptide concentration. This first step is promoted by the concentration gradient of peptide molecules in the early stage of the process [61,62]. The diffusion rate of peptide molecules towards the interface can be described by [63]:

$$\Gamma = 2C(Dt/3.14)^{1/2} \quad (7)$$

where D is the diffusion coefficient and Γ the surface concentration of the peptide at time t. To give an order of magnitude, the D values are 9.5×10^{-5} and 3.5×10^{-5} cm^2/min. for the α-helical $(LKKL)_4$ and the β-sheet $(LK)_8$ model peptides, respectively [64]. As stated above, there is initially no energy barrier to adsorption and the rate of arrival of molecules at the air/water interface is diffusion-controlled, therefore π and Γ change at the same rate and the measurement of π as a function of time allows the adsorption kinetics to be determined by applying the following first-order equation [65]:

$$\ln[(\pi_\infty-\pi_t)/(\pi_\infty-\pi_0)] = -Kt \quad (8)$$

where π_∞, π_t and π_0 are the surface pressures at the plateau, at time t and at zero time and K is the rate constant. $(\pi_\infty-\pi_0)$ called $\Delta\pi_\infty^{AW}$, is the maximum increase in surface pressure induced by the adsorption of a peptide (at a given concentration) at a clean air/water interface. As seen in Fig. 2b, in the case of defensin A the plot presents a slope change defining two rate constants $K_1 = 6\times10^{-3}$ min^{-1} and $K_2 = 4\times10^{-2}$ min^{-1} [66] values in the range of those found for various other proteins [65,67].

The surface activity of antimicrobial peptides is influenced by conformational factors, such as amphipathic structure, molecular size, molecular flexibility and net charge.

3.1. Influence of the primary sequence

The amphipathic character of a given peptide is a consequence of its amino acid sequence. As seen in Table 1, melittin and δ-lysin possess a highly asymmetrical polar/non-polar amino acid distribution with a cluster of six polar (including four cationic)

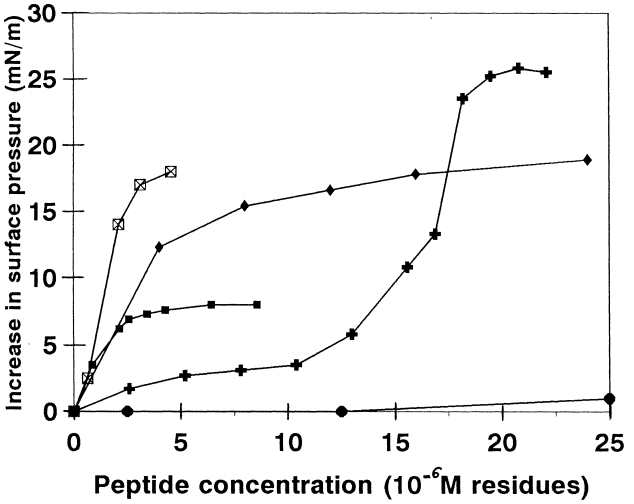

Fig. 3. Adsorption of some antimicrobial peptides at the air/water interface. Maximum increase in surface pressure ($\Delta\pi_\infty^{AW}$) versus peptide concentration in the subphase. ⊠, melittin in 0.145 M NaCl pH 5.6 (data from [73]); ♦, defensin A in 30 mM Tris buffer pH 7.6, 0.1 M KCl, T=20°C (data from [66]); ●, androctonin in 10 mM Tris buffer, pH 7.4, 0.1 M NaCl, T=20°C (unpublished results); ■, cardiotoxin isolated from *Naja naja oxiana* in 0.1 M KCl (data from [69]); +, δ-lysin (composition of the subphase unspecified) pH 6.8, T=22°C (data from [82]).

amino acids at the C-terminus in the case of melittin. On the contrary, non-polar amino acids are distributed all along the sequence of defensin A, bombolitin or cardiotoxin. As for androctonin, which possesses a high content in polar, including eight cationic, residues, it is an only slightly amphiphilic peptide, and, as shown in Fig. 3, it exhibits a very low surface activity. The influence of the primary sequence of antimicrobial peptides upon adsorption is well demonstrated in the case of the four cardiotoxins isolated from *Naja mossambica mossambica*, the sequence of which does not differ to a great extent [28]. Bougis et al. [68] have shown that, for the same concentration, 6×10^{-5} M(res)[2] in the subphase, the surface pressure increase varies from 6 mN/m for CTX II and CTX III to 9 mN/m for CTX IV and to 11 mN/m for CTX III RM. In the same way, Ksenzhek et al. [69] indicated that the *N*-acetylated toxin is more surface

[2] In order to compare the properties of the various antimicrobial peptides, all the concentrations will be expressed as mole of amino acid residue, i. e. M(res).

active than the native cardiotoxin from *Naja naja oxiana*. Antimicrobial peptides are polyelectrolytes and the presence of cationic residues might have a great influence on their adsorption behavior. In spite of this, Schröder et al. [70] have found an unchanged surface activity upon removing the hydrophilic and highly cationic (21–26) hexapeptide to the native melittin. However, it is likely that, although the adsorption extent remains the same, the adsorption kinetics changes in the absence of repulsive forces arising from the charged residues. Nevertheless, the Schröder finding indicates that, as a first approximation, the energy of adsorption would be determined primarily by the non-polar amino acid residues.

3.2. Influence of the tridimensional structure

The molecular size of peptides depends not only upon their sequence length, but mainly upon their tridimensional structure in solution (see in Fig. 4 the tridimensional structure of some antimicrobial peptides). In aqueous solution, the melittin monomer adopts a predominantly random-coil structure, whereas the tetramer is rich in α-helix [71]. In the tetrameric form, melittin has the conformation of a bent α-helical rod which exhibits a distinctive orientational segregation of hydrophilic and hydrophobic side chains, the latter being oriented mainly towards the inside of the helix bend [72]. The strong surface activity of melittin [73] can be therefore related mainly to its tridimensional structure as an assembly of amphipathic α-helices. Cardiotoxins, mammalian defensins or insect defensins are compact molecules rigidified by disulfide bridges which generally fold in such a manner that hydrophobic patches are created at the surface of the molecule. Cardiotoxins are able to adopt a three-fingered β-strand structure which presents an important hydrophobic region located at the tip of loop 1, in the middle of loop 2 and along a portion of loop 3 [74,75]. The structure of mammalian defensins, such as HNP-3, is dominated by a three-stranded antiparallel β-sheet self-associated as an amphipathic dimer [49]. Defensin A consists of three distinct domains: a N-terminal flexible loop, a helical fragment connected via two S–S bridges (16–36, 20–38) to an antiparallel two-stranded β-structure, the overall fold being stabilized by a third (3–30) S–S bridge. At the surface of the structured defensin A molecule, three hydrophobic patches are visible [23]. Conversely, the twisted β-hairpin structure of androctonin presents, mainly at the C-terminus, hydrophobic zones of only reduced stretch [76] and, as a result, it exhibits a low surface activity.

3.3. Unfolding of antimicrobial peptides upon adsorption at the air/water interface

Molecular flexibility is also an important factor for protein or peptide adsorption since, unlike other surfactants, these molecules tend to unfold at the interface, mainly at low surface pressures, in such a manner that their conformation is consistent with the maximum lowering of the surface free energy. Such a conformation will allow the maximum number of hydrophilic side groups to be oriented into the subphase and most of the hydrophobic ones to be projected away from the aqueous phase. It is generally admitted that secondary structures (α-helices and β-sheets) are preserved in the course of protein adsorption at the air/water interface [77]. This assumption has been demonstrated by spectroscopic analysis of transferred α-helical and β-sheet polypeptide monolayers by the technique of Langmuir–Blodgett [78]. Therefore, it is likely that melittin amphiphilic α-helices are adsorbed at the air/water interface without noticeable unfolding. Conversely, the CD spectrum recorded for defensin A transferred monolayers indicates a loss in the α-helix content (7%) as compared to that (20%) found in solution [79]. As a matter of fact, although the defensin A structure is rigidified by three disulfide bridges, it possesses a flexible N-terminal loop (residues 4–14) able to unfold at the air/water interface and containing one of the hydrophobic regions [23]. According to the protein adsorption model of MacRichtie [62] and as suggested by the sigmoidal aspect of the ($\Delta\pi^{AW}$–t) plot (Fig. 2a), the defensin A adsorption may be a cooperative process, the adsorption of one hydrophobic patch being the first step leading other hydrophobic parts of the peptide up to the interface.

The complete denaturation of δ-lysin in concentrated urea leads to a very high adsorption [80] probably because, in the absence of structural constraints, most of the amino acid residues are located at the interface.

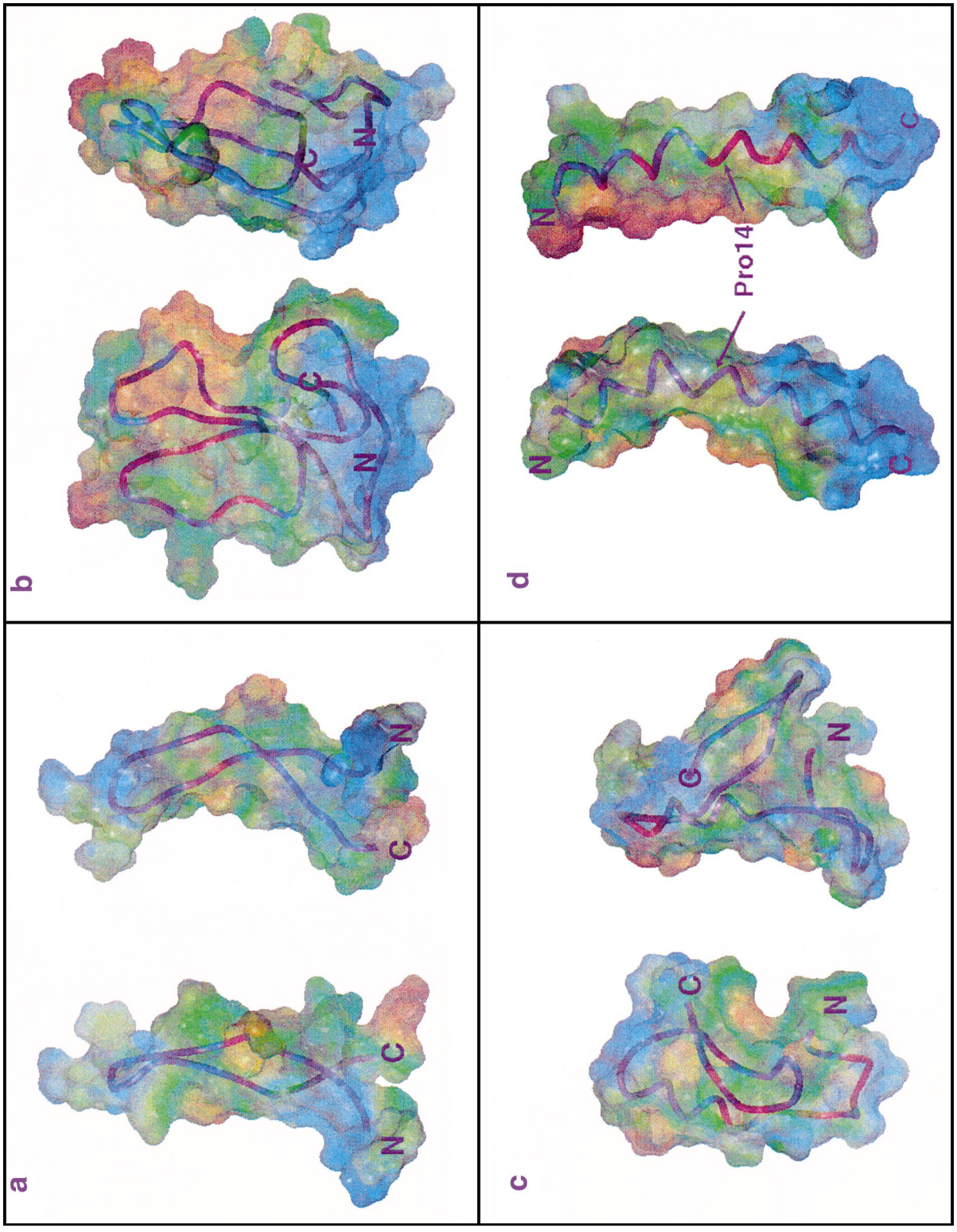
b
C
N
C
N
d
N
C
Pro14
N
C
a
C
N
C
N
c
C
N
C
N

Fig. 4. Tridimensional structure of some antimicrobial peptides. Hydrophobic potential surfaces MOLCAD (Sybyl-Tripos, Saint-Louis, MO, USA): from blue (hydrophilic) to brown (hydrophobic). Orthographic views of: (a) androctonin, Protein Data Bank ID code 1 CZ6 [76]; (b) cardiotoxin from Taiwan Cobra (*Naja Naja Atra*), Protein Data Bank ID code 2 CDX [75]. Note the three loops in the tube representation; (c) defensin A, Protein Data Bank ID code 1 ICA [23]; (d) melittin, Protein Data Bank ID code 2 MLT (M. Gribskov, L. Wesson, D. Eisenberg, 1990). Note the bend of the α-helix and the high hydrophilicity of the C-terminal part.
←

3.4. Influence of the subphase bulk composition

The adsorption of proteins or peptides from solution to interface is influenced by variables such as concentration, ionic strength, pH and temperature [81]. The influence of the peptide concentration in bulk upon adsorption is shown in Fig. 3 for some antimicrobial peptides at comparable ionic strength. The plateau in the ($\Delta\pi_{\infty}^{AW}$–C) plot corresponds to the saturation of the interface by the adsorbed peptides. The higher the pressure value at the plateau, the greater the surface-active properties of the peptide. We can see that the amphipathic helices, melittin and δ-lysin, are the most surface active and, conversely, the very hydrophilic androctonin is the least active in this concentration range. Increasing the bulk peptide concentration also favors self association. In the case of δ-lysin [82], the adsorption enhancement up to 10^{-5} M(res) (Fig. 3) may correspond to the formation of amphipathic aggregates. Colacicco et al. [80] reported a very low adsorption of δ-lysin when dissolved in distilled water ($\Delta\pi_{\infty}^{AW} < 1$ mN/m at $C \sim 8 \times 10^{-6}$ M(res)) as compared to the value reached in a buffer subphase. Likewise, increasing the ionic strength of the subphase results in an enhancement of both the adsorption rate and the extent of the defensin A adsorption [66]. The adsorption of charged peptides is maximum when the subphase pH is near their isoelectric point, thus avoiding electrostatic repulsion between already adsorbed peptides and peptides in solution.

4. Spread monolayers of antimicrobial peptides at the air/water interface

Another way to obtain a peptide film is to spread a peptide solution at the air/water interface. Conversely to monolayers resulting from adsorption and which are in equilibrium with molecules in the bulk phase, spread monolayers are in a metastable state. Peptides are generally spread by carefully adding a small amount of a concentrated aqueous solution at the air/water interface, with a microsyringe. Our personal method is to dilute the aqueous peptide solution with a given amount of a volatile solvent (hexafluoroisopropanol) miscible with water. The surface area to volume ratio of the trough must preferentially be higher than 1 cm^{-1}.

Owing to the high hydrosolubility of most antimicrobial peptides, the hypothesis of a total absence of desorption of the spread peptide into the subphase must be verified. Schwartz and Taylor [83] have elaborated a pertinent thermodynamic analysis to evaluate the partition of a spread peptide between the monolayer and the subphase. In each experiment the surface pressure, π, is measured with a given amount, n_s, of spread peptide for a gradually decreasing trough area, s. A series of π versus s isotherms are recorded using a number of sufficiently different values of n_s. Then pairs of n_s and s taken from all the available isotherms at the same surface pressure are collected. Because of mass conservation, these quantities must obey the relation:

$$n_s = \Gamma s + VC \tag{9}$$

where Γ is the surface concentration of the peptide, V is the volume of the subphase and C is the peptide concentration in the subphase.

Thus, plotting n_s as a function of s gives a straight line with a slope equal to Γ, and C can be determined from the intercept with the ordinate. From this analysis it is possible to show clearly any peptide desorption from the spread monolayer.

4.1. General properties of spread monolayers [53,54]

The main parameters which characterize the film state of a given substance spread on an aqueous subphase are the temperature T, the surface pressure π, the surface area and the number of molecules, these

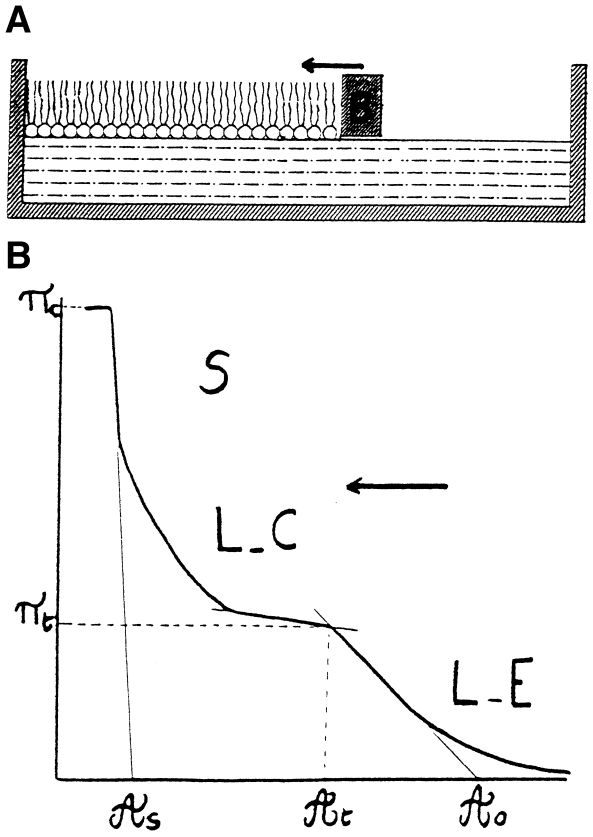

Fig. 5. (a) Schematic representation of a Langmuir balance experiment. B is the movable barrier. The arrow indicates the direction of the barrier when the film is compressed. (b) Compression isotherm of a monolayer: L-E, liquid-expanded state; L-C, liquid-condensed state; S, solid state; π_c, collapse pressure; π_t, transition pressure (at the beginning of the L-E–L-C transition); A_t, mean area at π_t; A_0, limiting area; A_S, area in the solid state. The arrow indicates the direction of the compression.

two last parameters being expressed as area per molecule, A.

Therefore, at constant T, an equation of state of the film has the general form:

$$\pi = \pi(A)_T$$

The surface pressure–area (π–A) isotherm of a monolayer constitutes the essential characterization of the properties of the film although surface potential measurements, which give information regarding the orientation of the film constituents, are also usually performed.

4.1.1. The Langmuir film balance

Surface pressure–area (π–A) isotherms are often carried out by means of a Langmuir film balance (Fig. 5a). The original Langmuir method was based on directly measuring the outward horizontal force exerted on a floating barrier that divides the film covered surface from a clean surface. The spread monolayer can be compressed by means of a movable barrier while the surface pressure and the area are continuously recorded. Surface potential–area (ΔV–A) isotherms are also recorded, usually in conjunction with (π–A) isotherms. In recent versions the trough and the barriers are often made of Teflon. The whole device rests on an antivibration plate and is placed inside a thermostated box.

4.1.2. States of monomolecular films

In course of the film compression, there is a change in the molecular packing. The compression rate must be slow enough to ensure that changes occur under thermodynamic equilibrium conditions (in our experiments, spread peptide monolayers were compressed by means of a step by step motor at a rate varying between 0.2 and 2 Å^2/amino acid

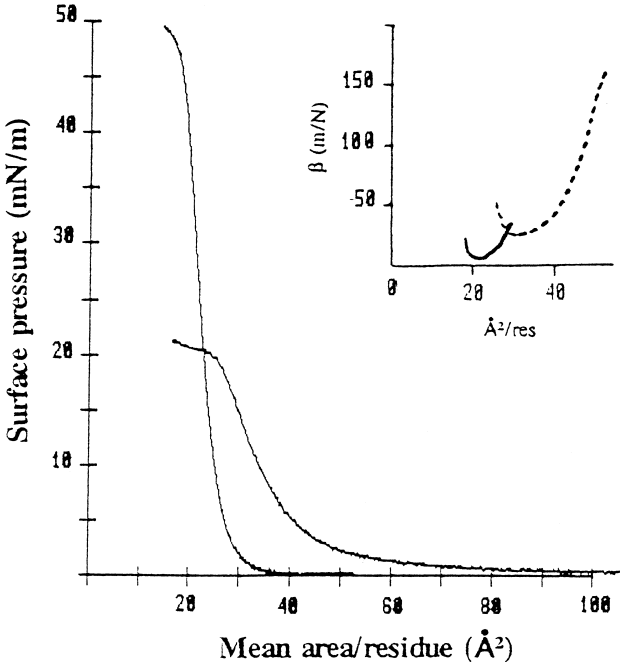

Fig. 6. Compression isotherms of $(LKKL)_4$ (right) and $(LK)_8$ (left) spread monolayers [64]. Inset: corresponding compressibility coefficient as a function of the area/residue. ——, $(LK)_8$; - - -, $(LKKL)_4$ (unpublished data). Subphase: 0.1 M KCl; T = 20°C.

residue/min). The variations of the surface pressure of a film with the area imply some degree of elasticity of the monomolecular film. The equilibrium elasticity is related to the compressibility of the film defined by the *compressibility coefficient* $\beta = -1/A(\partial A/\partial \pi)_T$ (see inset to Fig. 6 as an example). Surface pressure–area isotherms are analogous to three-dimensional P–V isotherms although the correspondence is not complete. A schematic representation of monolayer states is given in the Fig. 5b. When the molecules are sufficiently far apart for lateral cohesion forces (van der Waals forces) to be negligible, the film is in the gaseous state.

The ideal gas film obeys the relationship:

$$\pi A = kT$$

where k is the Boltzmann constant.

In liquid films, there is some degree of cooperative interaction between molecules. Liquid-expanded (L-E) films are very compressible and the π–A plot extrapolates at $\pi = 0$ to an area called *limiting area*, A_0. It is often of interest to calculate $\beta_0 = -1/A_0(\partial A/\partial \pi)_T$, the compressibility coefficient at A_0. In liquid-condensed (L-C) films, molecules begin to be close-packed. There is generally a transition region of higher compressibility between L-E and L-C states which begins at the *transition pressure* π_t and the corresponding area A_t. Solid films are characterized by a low compressibility and the π–A plot extrapolates to zero π at an area, A_s, near the molecular cross section. On further compression the film collapses in a three-dimensional state at the *collapse pressure* π_c (see Fig. 5b for the definition of the various parameters).

4.1.3. Equation of state of spread protein or peptide monolayers [84] and analysis of their π–A isotherms

The behavior of proteins at interfaces is mainly determined by their predominant secondary structures which are mainly α-helix and β-sheet. Comparative π–A isotherm characteristics of model peptides in α-helical, β-sheet and random coil structures have been described [64,85]. β-Sheet peptides form stable monolayers in a condensed state which collapse at a high surface pressure (π_c near 50 mN/m) and the limiting area is between 18 and 25 Å^2/res [3]. Monolayers of α-helical peptides are more compressible and less stable (the collapse pressure ranges generally between 20 and 30 mN/m) and A_0 may reach 50 Å^2/res (see Fig. 6).

An equation of state for protein or peptide monolayer is obtained by applying the general equation of state for amphiphiles,

$$\pi = \pi_{kin} + \pi_{el} + \pi_{coh} \quad (10)$$

where π_{kin} arises from the kinetic movement of the film, π_{el} from the electrostatic repulsion between charged residues and π_{coh} from the van der Waals forces between the apolar side chains.

$$\pi_{kin} = kT/A \text{ (ideal film)}$$

According to the Gouy–Chapman model, the term π_{el} is given by

$$\pi_{el} = \int_0^{\Psi_0} q \, d\Psi$$

where q is the charge density at the interface and Ψ_0 is the average electrical potential in the plane of monolayer arising from the polar groups of the film forming molecules (see Eq. 6).

The quantitative expression of π_{el} is derived as (equation of Davies):

$$\pi_{el} = 6.1 \sqrt{c} \, [\cosh \sinh^{-1} (134z/A\sqrt{c}) - 1] \quad (11)$$

where c stands for the concentration of monovalent counterions in the subphase and $z = qA$ for the number of charges per spread molecule.

At low surface pressure ($\pi < 1$ mN/m) the cohesive forces are negligible as compared to the term π_{el}. Therefore the equation of state for charged peptide or protein monolayers at low surface pressure becomes:

$$(\pi - \pi_{el})(A - a_0) = kT \quad (12)$$

where a_0 is a parameter named *coarea* which corrects for the area actually occupied by a molecule.

From Eq. 12, it can be seen that plotting πA versus π results in a linear relation with a slope a_0 and an intercept with the ordinate axis equal to $\{\pi_{el}(A - a_0) + kT\}$. At the ordinate intercept, $\pi \rightarrow 0$ and then $A \rightarrow$ the area at the liftoff of the isotherm.

[3] The interfacial molecular area of the various peptides will be generally expressed as Å^2/amino acid residue, i.e. Å^2/res.

When the experimental value found at the ordinate intercept differs from the theoretical (calculated) value, this discrepancy is generally attributed to a molecular aggregation in the film [54] with an aggregation number n_{ag} = (calculated value)/(value at the intercept). Applying this method to the $(LKKL)_4$ and $(LK)_8$ isopeptides, we concluded that the β-sheet peptide has a higher degree of self association at the air/water interface than its α-helical isomer [64]. This finding agrees with the situation encountered in solution where β-sheet peptides have a greater tendency than α-helix peptides to form aggregates because the hydrogen bonds in β-sheet are arranged between one strand and another with a thermodynamic preference for the antiparallel structure [86].

According to Birdi [87], it is possible to estimate the degree of unfolding of proteins at the air/water interface from their π–A isotherms. He suggested that the wider the difference between the work of compression and the work of expansion, the more important the degree of unfolding of the protein. This statement is valid provided that no loss of protein into the subphase occurs in the course of the compression. It is therefore better to stop the compression well before the collapse of the monolayer when recording a compression–expansion cycle.

The work of compression (or of expansion) is given by:

$$W = \int_{\text{initial}}^{\text{final}} \pi \mathrm{d}A$$

4.2. *Spread monolayers of gramicidin A and its analogs*

Gramicidin A (GA) monolayers have been studied by several authors [88–91]. The shape of their compression isotherm (Fig. 7) is consistent with that of hydrophobic α-helical compounds [92]. At low pressures, gramicidin A forms compressible monolayers with a limiting area $A_0 \sim 25$ Å^2/res compatible with a side by side horizontal orientation of the helices. The isotherm shows an inflection around 11 mN/m, which indicates the beginning of a transition. This transition corresponds probably to an interdigitation of the helices, in agreement with the analysis of Lavigne et al. [92], but certainly not to the collapse of the monolayer as asserted by Davion-Van Mau et al.

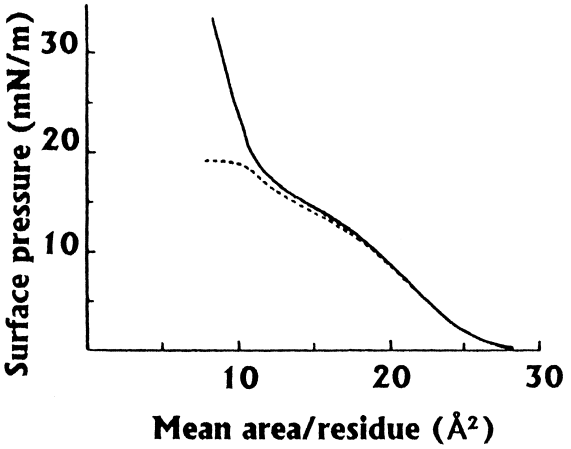

Fig. 7. Compression isotherms of gramicidin A monolayers spread on a 10 mM Tris-Cl, pH 7.4 subphase; T = 20°C. ——, isotherm recorded upon continuous compression; - - -, isotherm recorded upon stepwise compression and relaxation. Data from [90].

[89]. Continuing compression results in a steep increase in surface pressure and the monolayer becomes highly incompressible. The extrapolated area, $A_s \sim 10$ Å^2/res (i.e. 150 Å^2/molecule) agrees with an orientation of gramicidin A perpendicular to the interface [93]. The hypothesis of an orientation change during the compression is supported by the results of conformational analysis done by Brasseur et al. [94]. As a matter of fact, these authors reported the existence of two types of organization within gramicidin A aggregates, at the air/water interface: a linear organization (corresponding to α-helices oriented parallel to the interface) and another in a perpendicular orientation leading to tubular structures. However, a collapse pressure of only 18 mN/m has been determined by Tournois et al. [90] by stepwise compression and relaxation of the monolayer. This result suggests that, when monolayers are compressed in thermodynamical equilibrium conditions, gramicidin A molecules stay in a parallel orientation with a progressive interdigitation of the α-helices and thus the collapse may correspond to the formation of a bilayer [95]. Adding KCl to the subphase does not result in a modification of the isotherm [88] in accordance with the hydrophobic nature of gramicidin A.

The interfacial properties and the conformational behavior of gramicidin A at the air/water interface are not affected when various acyl chains are cova-

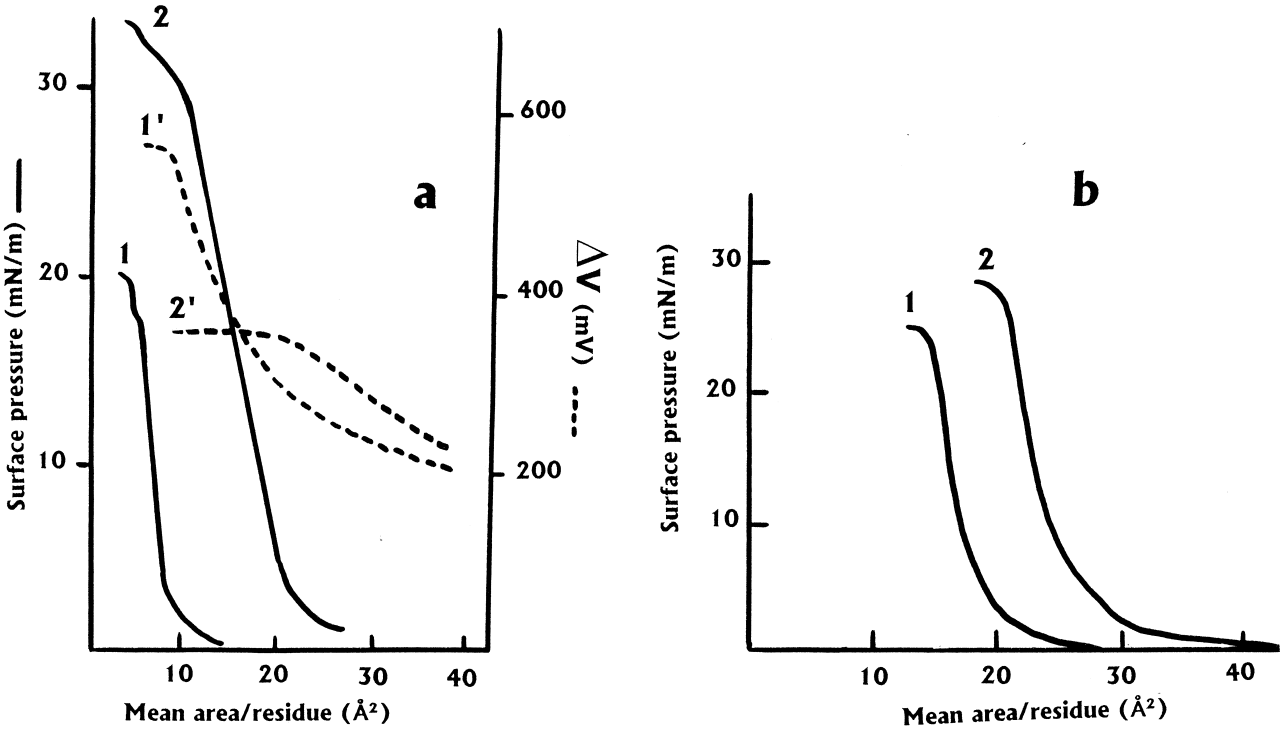

Fig. 8. Compression isotherms: —— (π–A) and - - - (ΔV–A) of (a) melittin monolayers spread on a water subphase (1 and 1′) and on a 1 M KCl subphase (2 and 2′); T = 25°C. Data from [102]. (b) bombolitin monolayers spread on water (1) and on 10 mM Tris, 20 mM NaCl, 0.5 mM $CaCl_2$, pH 8 (2); T = 25°C. Data from [100].

lently coupled to the C-terminal ethanolamine group [96]. When highly compressed, the acyl-gramicidin molecule would be oriented with its C-terminus towards the subphase and the coupled acyl chain located parallel to the helix axis in between the protruding tryptophans. The nature of the aromatic residue appears to be essential for the channel function of gramicidin A [97]. For this reason, Davion-Van Mau et al. [89] synthetized analogs of GA where all Trp residues were replaced by Tyr giving GT, Phe giving GM$^=$ or Tyr-(OBzl) giving GT′. GT and GM$^=$ monolayers are less compressible than GA or GT′ monolayers because their side chains are shorter, and the transition occurs at higher pressures (21–22 mN/m). Also, changing only one Trp residue alters the interfacial properties of GA. For example, the [Phe-9] analog monolayer is more condensed ($A_0 \sim 20$ Å^2/res instead of 25 Å^2/res) than the GA monolayer, and its isotherm lacks a transition region [89]. Conversely, analogs in which the central region is extended by two hydrophobic residues (Leu-Ala) have comparable isotherm characteristics to those of GA monolayers [90]. The active structure of gramicidin A being a head to head dimer [50], Davion-van Mau et al. [89] synthetized a covalent retro GA-D Ala-GA dimer. Although the transition occurs at the same pressure ($\sim$11 mN/m), the monolayers of GA-D Ala-GA are more condensed ($A_0 \sim 18$ Å^2/res) than GA monolayers suggesting that the dimer adopts a different conformational state than gramicidin A [89].

From surface potential measurements it appears that gramicidin analogs can be classified into two groups: for the first group (GA and GT), ΔV is around 200 mV at the plateau of the (ΔV–A) isotherms (when the monolayer is highly compressed), whereas for the second group (GM$^=$ and GT′) ΔV reaches more than 300 mV. It was suggested that a correlation may exist between surface potential values and single channel behavior. As a matter of fact, the channel conductance units of GA and GT are high and almost independent of the applied voltage whereas those of GM$^=$ and GT′ are lower and strongly voltage dependent [89].

4.3. Spread monolayers of melittin, bombolitin III and δ-lysin

Structured as amphipathic α-helices, melittin [59,73,98,99] and bombolitin III [100] as well as δ-lysin [80] form stable monolayers at the air/water interface. From the partition analysis of spread melittin molecules between the monolayer and the subphase, Wackerbauer et al. [101] concluded, by applying Eq. 9, that melittin molecules manifest a strong preference for an accumulation at the air/water interface. However, at high surface pressure (about 30 mN/m) an appreciable degree of melittin desorption occurs, attributed to the excessive mutual repulsion of melittin molecules which limits their surface concentration. On a pure water subphase, melittin monolayers (Fig. 8a) are in a very condensed state and the A_0 value ($\sim$8.5 Å^2/res) is far from corresponding to that of an α-helix lying flat at the interface [102]. The reason may be the presence of a bend at Pro-14: the 15–26 hydrophilic C-terminal peptide may be fully hydrated while the more hydrophobic N-terminal part points away from the aqueous phase. In such a situation the 15–26 C-terminal peptide adsorbed at the interface of the water subphase is in a medium of dielectric constant $\varepsilon = 78$ while the N-terminal part is in a medium of dielectric constant $\varepsilon = 1$ and the cationic Lys-7 is not able to fully interact with the aqueous phase. This could explain why the (π–A) isotherms of melittin monolayers spread on a water subphase cannot be analyzed by using the Gouy–Chapman model which does not take sufficiently into account the effect of the medium dielectric constant [59]. As seen in the Fig. 8b and in contrast to melittin, the value of A_0 ($\sim$20 Å^2/res) of bombolitin III on a water subphase [100] is compatible with a horizontal orientation of the helix part of the peptide (the α-helix content of bombolitin III being 60–70%). The collapse pressure ($\sim$25 mN/m) of bombolittin III monolayers is within the same range as that (20 mN/m) of melittin monolayers, but lower than that (40 mN/m) of δ-lysin monolayers under the same experimental conditions [80].The higher stability of δ-lysin monolayers may result from the less net charge of the peptide. The addition of KCl in the subphase enhances the stability of both bombolitin III and melittin monolayers which collapse pressure and limiting area become higher

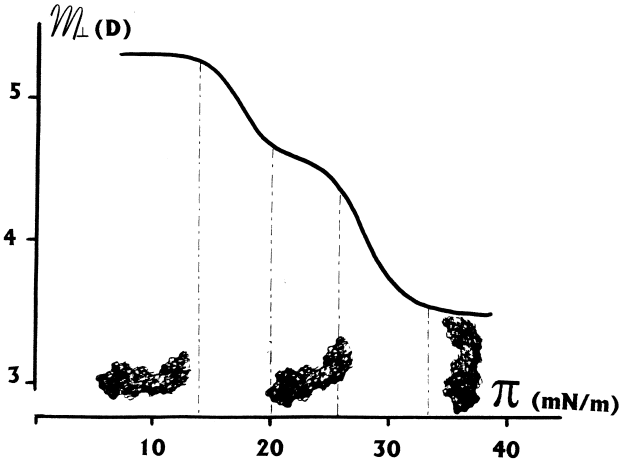

Fig. 9. Interfacial dipole moment per melittin molecule as a function of surface pressure. The successive states (orientations) of the melittin molecules correspond to $\mathcal{M}_\perp = 5.3$ D, 4.6 D and 3.5 D, respectively. Subphase: 60 mM citrate buffer, pH 7; $T = 23 \pm 1$°C. Data from [101].

(Fig. 8). The collapse pressure of melittin monolayers reaches 30 mN/m on 1 M KCl and the (ΔV–A) isotherms (Fig. 8a) indicate that the corresponding value of ΔV goes from 580 mV on a water subphase to $\sim$400 mV on 1 M KCl [102]. Concurrently, A_0 attains 22.5 Å^2/res, a value now in agreement with a horizontal orientation of the α-helices, an orientation recently demonstrated unambiguously by Wackerbauer et al. [101] from surface potential measurements. These authors showed that well-pronounced transitions of the effective dipole moment $\mathcal{M}_\perp$ occurred in the course of the compression (Fig. 9). At low surface pressure ($\pi < 13$ mN/m) the molecules adopt a parallel orientation with an interfacial area varying from 23 to 15 Å^2/res. Then they undergo a transition towards a state corresponding to a straightening-up process of the α-helices. At last, up to 30 mN/m, $\mathcal{M}_\perp = 3.3$ D and $A \sim 10$ Å^2 in good agreement with a vertical orientation of the melittin molecules. Fidelio et al. [103] reported that, curiously, the isotherm shape of melittin monolayers on saline subphase (0.145 M NaCl) is similar over a wide range of temperature (5–40°C), whereas it is sensitive to the subphase pH. On alkaline subphase, the melittin monolayers are more condensed and more stable, as attested by the collapse pressure increase (from 20 mN/m at pH 5.6 to 28 mN/m at pH 10.6). Nevertheless, according to Wackerbauer et al. [101], in-

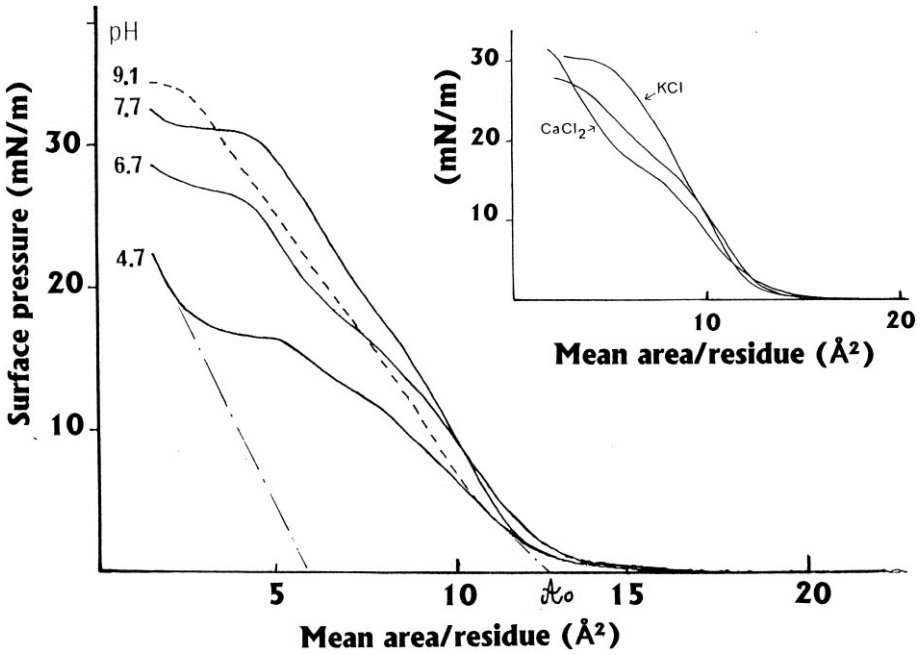

Fig. 10. Compression isotherms of defensin A spread on 30 mM Tris-Cl subphases at various pH. A_0 is the limiting area of defensin A on a pH 4.7 subphase; to compare with the extrapolated value from the condensed part of the isotherm. Inset: defensin A isotherms recorded on a 30 mM Tris-Cl, pH 7.2 subphase (center) or containing either 100 mM KCl or 2 mM $CaCl_2$; $T = 20°C$. Data from [66].

creasing the pH apparently favors the melittin partition into the subphase.

From the analysis of the πA versus π plot, according to Eq. 12 and giving $(\pi A)_{\pi \to 0} = kT/4$, Gevod and Birdi [104] concluded that melittin is present as a tetramer at the interface. Given the low value of A_0, the melittin tetramer may be oriented vertically with the polar end (20–26 residues) situated in the aqueous phase. However, this is a very controversial result since, on the one hand, De Grado et al. [98] reported that melittin is in a monomer state at the air/water interface and, on the other hand, Terwilliger et al. [72] suggested, on the basis of crystallographic studies, that a melittin monolayer is constituted by a dimer layer.

4.4. Spread monolayers of defensin A [66]

Defensin A monolayers were spread from a (water/methanol/hexafluoroisopropanol 1:3:4, v/v/v) solvent mixture. Isotherms of defensin A monolayers at various pH subphases are shown in Fig. 10. The value of the limiting area $A_0 = 12$–13 Å^2/res indicates that the peptide is only partially unfolded at the interface, due to the presence of the three disulfide bridges. The wide hysteresis observed in the course of the compression–expansion cycles (not shown) was mainly attributed to a reversible desorption of the molecules just below the interface. On acidic subphases, there is a steep increase in surface pressure after the plateau. In this region, the extrapolated area at $\pi = 0$ is ~ 6 Å^2/res, a value about half the A_0 value, suggesting a bilayer organization of the defensin A film. Therefore, the plateau would represent the monolayer–bilayer transition. When the subphase pH increases, the defensin A monolayers become more stable: π_c increases from 16 mN/m at pH 4.7 to 34 mN/m at pH 9.1 and the (π_c–pH) plot shows a plateau beginning around the isoelectric point (p$I \sim 8.3$) of defensin A in solution, conditions in which the peptide exhibits its maximum hydrophobicity. Concurrently, defensin A monolayers become less compressible (β_0 goes from 32 to 22 m/N) and the transition region gradually vanishes. Given the constant A_0 value, it can be supposed that, at low pressures, defensin A molecules maintain more or less the same orienta-

tion. The addition of 0.1 M KCl in the subphase leads to similar features to basic pH, probably as the result of a screening effect. The addition of only 2 mM $CaCl_2$ induces significant changes in the shape of defensin A monolayers. The transition region is now more pronounced and the liquid–condensed region of the isotherm is less compressible (see Fig. 10 inset). These features were attributed to the binding of Ca^{2+} ions to defensin A molecules at the level of Asp-4 and/or of the terminal COO^- group, with possible Ca^{2+} bridges between adjacent defensin A molecules promoting the formation of dimers.

5. Penetration of antimicrobial peptides into lipid monolayers

5.1. Lipid monolayers as membrane models

With the aim of studying interactions between a given effector (antimicrobial peptide, for instance) and cell membranes, several approaches are possible. We can work with living cells and observe what happens in situ or we can isolate cellular membranes. However, natural membranes are very complex entities with a great variety of lipids and proteins, thus, in this case, we can only investigate global phenomena. Therefore, if we are interested in specific aspects of a given biological phenomenon occurring at membrane level, the best choice is to use membrane models. Among them, bilayer lipid membranes (BLM) are the most suitable for the study of ion transport across membranes [105]. Lipid vesicles (SUV, LUV or multilamellar), a widely used model [106], possess an internal aqueous compartment and are also suitable for permeability studies. However, although lipid vesicle experiments are easy to carry out and allow various spectroscopic measurements, the lipid vesicle system presents some disadvantages. Firstly, it is not always possible to prepare vesicles: with pure phosphatidylethanolamine, for example, either with 100% charged lipid or containing more than 50% cholesterol or at a temperature less than the gel–liquid crystal transition temperature of the phospholipids. Furthermore, it is difficult to prepare a homogeneous (in size and in layer number) vesicle suspension and to avoid spontaneous fusion. Another disadvantage

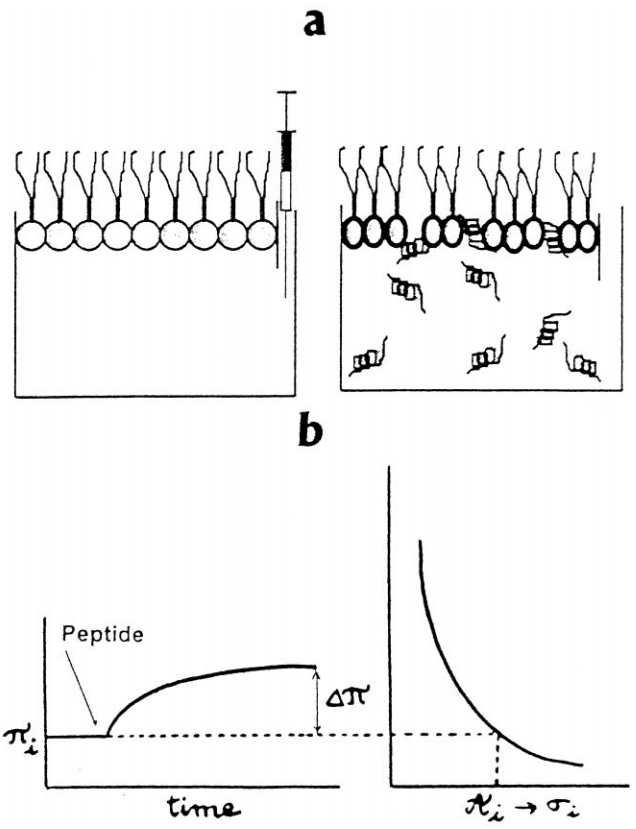

Fig. 11. (a) Schematic representation of a penetration experiment: injection of a peptide solution beneath the lipid monolayer (left) and insertion of peptide molecules into the lipid monolayer (right). (b) Definition of various parameters extracted from penetration experiments: surface pressure increase (from π_i to $\pi_i+\Delta\pi$) of the lipid monolayer upon injection of a peptide solution (left); determination of the initial density, σ_i, of the lipid monolayer from the π–A isotherm curve (right).

is the small curvature radius of vesicles that imposes strong constraints at the polar head level.

On the contrary, with the monolayer system, a number of parameters including the nature and the packing of the lipid molecules, the composition of the subphase and the temperature, can be chosen without any limitation. The interest of phospholipid monolayers as membrane models [107] consists also in their homogeneity, their stability and their planar geometry where the lipid molecules have a specific orientation. Besides, as seen before, this well-defined bidimensional system provides rigorous thermodynamic analysis. The lipid monolayer is also a very suitable model to study, in conditions near the actual

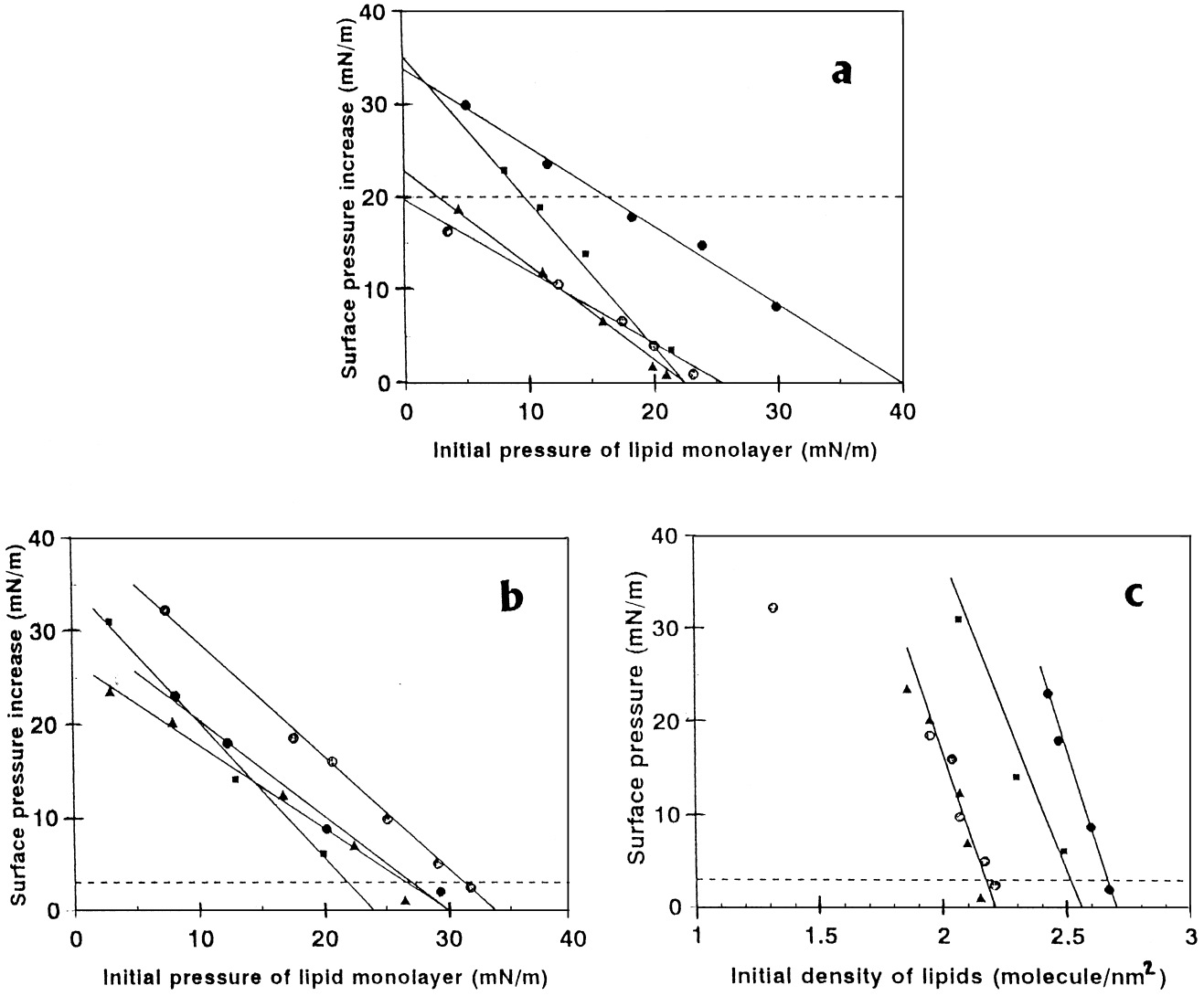

Fig. 12. Melittin and δ-lysin penetration into phospholipid monolayers. (a) Maximum increase in surface pressure ($\Delta\pi$) as a function of the initial pressure, π_i of the phospholipid monolayer, upon injection of 8.84×10^{-6} M(res) of melittin in the subphase. Data from [82]. (b) Maximum increase in surface pressure as a function of π_i upon injection of 8.84×10^{-6} M(res) of δ-lysin in the subphase. Data from [82]. (c) The same as in b, but $\Delta\pi$ is plotted as a function of the initial density σ_i of phospholipids. Data calculated from [82] and [115]. ○, DPPC; ▲, DPPE; ■, DPPA; ●, DPPG. Pure water subphase, pH 6.8; $T=22$°C. The dotted lines represent the maximum value of surface pressure, $\Delta\pi_\infty^{AW}$, induced by the peptide adsorption at a clean air/water interface in similar experimental conditions (see Fig. 3).

biological ones, what happens when a hydrosoluble peptide, present in the extracellular medium, arrives at the membrane surface of the target cell. Finally, in a recent article, Brockman [108] argued convincingly in favor of lipid monolayers over bilayers as a model to characterize protein–membrane interactions. For further details about bilayer and monolayer correspondence, see [109] and [110] as reviews.

5.2. *General considerations on the penetration of soluble compounds into spread insoluble monolayers [111]*

Generally speaking, the term 'monolayer penetration' is used to describe the interaction of an insoluble monolayer spread at the air/water interface with a soluble active compound present in the aqueous

phase. The interaction can be measured in two ways. The film pressure can be kept constant and the reaction followed by observing the increase in area of the film. The second method, by far the most widely used, is to maintain the film area constant and to measure the surface pressure changes on adding the penetrating compound to the subphase. Herein, the insoluble monolayer is a lipid monolayer and the penetrating compound an antimicrobial peptide. The experimental device generally consists in a small dish equipped with a vertical tube through which the peptide solution is injected (Fig. 11a). Lipid monolayers are formed at the required pressure by intermittent spreading of the lipid solution in the appropriate solvent mixture (containing generally chloroform and methanol). The parameters that must be taken into account are: (1) the initial pressure of the lipid film, π_i, which reflects the packing of the lipids in the monolayer. However, in order to compare the peptide penetration in various lipid monolayers, it is best to choose the lipid density, σ_i, as the lipid packing parameter (Fig. 11b); (2) the concentration, C, of the peptide in the subphase; (3) the maximum change, $\Delta\pi_\infty^{Lip}$ (called $\Delta\pi$ to simplify), in surface pressure of the lipid film upon interaction with the peptide dissolved in the subphase. As far as possible, C must be low enough for the surface pressure, $\Delta\pi_\infty^{AW}$, induced by adsorption of the peptide at a clean air/water interface (see Section 3) in the same experimental conditions, to be negligible. Otherwise, the result under consideration must be the *interaction pressure* $\Delta\pi_\infty^{Lip}-\Delta\pi_\infty^{AW}$. The lipid film pressure at which the peptide no longer penetrates is called the *exclusion pressure*, π_{ex} and, in the case of a $(\Delta\pi-\sigma_i)$ representation, an *exclusion density*, σ_{ex} is defined.

5.3. Penetration of δ-lysin and melittin into phospholipid monolayers

Bhakoo et al. [82] have studied the penetration of δ-lysin and melittin into various phospholipid monolayers. At the subphase concentration used, $C=8.84\times10^{-6}$ M(res), the adsorption of δ-lysin at a clean interface induces an increase in surface pressure of only 3 mN/m, but for melittin, $\Delta\pi_\infty^{AW}$ reaches $\sim$20 mN/m (Fig. 3). Thus, at this concentration, although melittin penetrates into all type of phospholipid monolayers, it interacts specifically only with acidic phospholipids (DPPG and DPPA) (Fig. 12a) in agreement with its highly cationic nature. In the same way, studying the area increase of DPPC and DPPG monolayers upon melittin injection, Hendrickson et al. [112] found also a greater peptide penetration into DPPG monolayers. Recently, by in situ infrared reflection (IRRAS) measurements at the air/water interface, Flach et al. [113] confirmed this finding and outlined that melittin interacts differently with zwitterionic compared with negatively charged monolayer surfaces. However, Ohki et al. [114] reported an opposite result with natural phospholipid monolayers (egg-PC and bovine PS), which, owing to the presence of unsaturated chains, are always in an expanded state even at high surface pressures. Melittin was also found to induce a greater area increase of DMPC with respect to DMPG monolayers [112]. These controversial results could be related to the length and the nature of the aliphatic chains. As a matter of fact dimyristoyl phospholipid monolayers do not exhibit L-E–L-C transition and are more expanded than the corresponding dipalmitoyl phospholipid monolayers [115]. Besides, a dramatic increase in melittin insertion at a π_i corresponding to the L-E–L-C transition of DPPC and DPPG was also reported [112]. Therefore, it can legitimately be thought that, in addition to the polar head nature (zwitterionic or acidic) of the phospholipids, the physical state of the lipid monolayer is involved in the penetration process. For instance, the bent α-helical structure of melittin could hinder a complete penetration into the rigid chains of DPPC or DPPE films, but not into the short expanded chains of DMPC. In addition, the charge of the lysine-7 residue prevents an integral insertion of the N-terminal hydrophobic segment of melittin [116]. But we must keep in mind that a weaker penetration into acidic phospholipid monolayers is not synonymous with a weaker binding. As a matter of fact, it has been clearly shown that melittin binds fluid negatively charged phospholipids intensively [117]. However, owing to their high positive net charge, the first bound melittin molecules exert a repulsive effect on the following ones. The first step of the penetration process is the peptide adsorption at the surface of the monolayer, which is known to induce only negligible changes in surface pressure. This happens in all

cases, and even with neutral phospholipid monolayers, at surface pressures higher than π_{ex}. For instance, Ebara and Okahata [118] have shown, by QCM experiments, that melittin adsorbs on DPPE monolayers at $\pi_i = 40$ mN/m, a pressure far above the exclusion pressure as seen in Fig. 12a. At the subphase concentration (10^{-6} to 2×10^{-5} M(res)) and in pH and ionic strength conditions generally used in monolayer experiments, melittin is in a monomeric state [34] and mainly in a random coil conformation [119]. Melittin undergoes conformational changes upon binding to phospholipid monolayers. From CD spectra analysis of transferred DMPA monolayers, Sui et al. [120] showed that inserted melittin (at $\pi_i = 15$ mN/m) contains more α-helix structure than adsorbed melittin (at $\pi_i > \pi_{ex}$). When adsorbed, the α-helix of melittin would lie with its axis parallel to the membrane surface [121] and its hydrophobic face directed toward the membrane interior [122]. However, from IRRAS measurements, Flach et al. [113] recently suggested that melittin adopts a conformation different from α-helix when bound to phospholipid monolayers.

Conversely to melittin, δ-lysin interacts specifically with all the phospholipids tested, as seen Fig. 12b. The exclusion pressure in DPPC monolayers reaches ~32 mN/m for δ-lysin whereas it is only 25 mN/m for melittin. The same observation can be made for DPPE, giving a further indication of the greater affinity of δ-lysin for zwitterionic phospholipids, as compared to melittin. The penetration power of δ-lysin into DPPG monolayers is lower than that of melittin since $\pi_{ex} = 31$ mN/m instead of 40 mN/m, probably because the net charge of δ-lysin is less. However, the exclusion pressure in DPPA monolayers is the same for both peptides. On the basis of the $\Delta\pi$–π_i plots, Bhakoo et al. [82] concluded that differences in the phospholipid head group have little effect on the degree of interaction between δ-lysin and the phospholipid film. However, plotting $\Delta\pi$ as a function of the initial molecular density, σ_i, obtained from the π–A isotherms of phospholipids [115], leads to the opposite conclusion. As a matter of fact, the $\Delta\pi$–σ_i plot (Fig. 12c) indicates that the penetration extent of δ-lysin into the various phospholipid films varies in the order: DPPC = DPPE < DPPG. The penetration profiles of δ-lysin in DPPC and DPPE are identical except at low DPPC density (corresponding to the expanded part of the π–A isotherm of DPPC before the L-E–L-C transition).

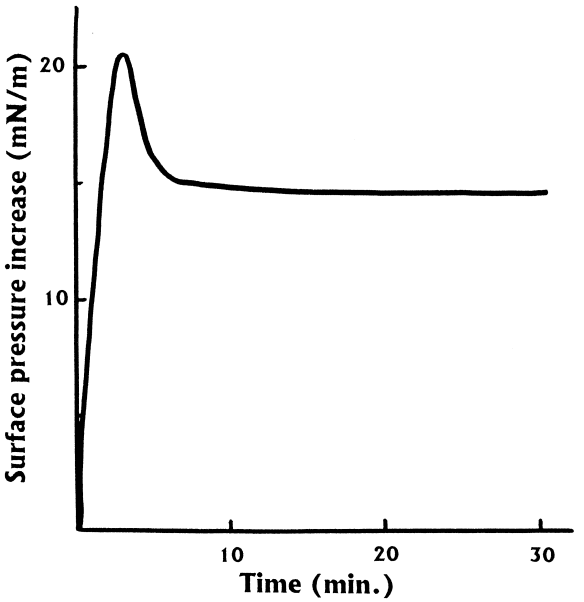

Fig. 13. Kinetics of surface pressure increase related to cardiotoxin (CTX III) penetration into a DLPS monolayer. CTX III concentration: 3×10^{-5} M(res). π_i of DLPS monolayer: 25 mN/m. Subphase: 20 mM Tris-acetate, pH 5; $T = 25$°C [68].

5.4. Penetration of cardiotoxins into phospholipid monolayers

As seen in Table 1 and Fig. 4, cardiotoxins are rigid molecules structured as three β-strand loops. Bougis et al. [68] found that cardiotoxins penetrate readily into DLPS (an acidic phospholipid possessing very short (C12) acyl chains) monolayers, but also into neutral phospholipid monolayers. At the subphase concentration (6×10^{-6} M(res)) used in these monolayer experiments, the surface pressure increase at a clean air/water interface, $\Delta\pi_\infty^{AW}$, varies roughly from 6 mN/m (for CTX I) to 11 mN/m (for CTX III RM). Therefore, apart for CTX III RM, the increase in surface pressure of DLPS monolayers reveals specific interactions with the various cardiotoxins. When the subphase is devoid of Ca^{2+} ions, the penetration kinetics presents a transitory phase of overpressure (Fig. 13). This feature was attributed by the authors to a condensation of the DLPS film, the positive charges of cardiotoxins substituting for Ca^{2+} ions. From the π_{ex} values (from 25 to 45 mN/m), the pen-

etration powers of the various cardiotoxins in DLPS monolayers are found in the order: CTX III RM ≪ CTX I = CTX II = CTX III ≪ CTX IV. Applying the Gibbs relation (Eq. 5) to the penetration of CTX III into a DLPS film, the apparent interfacial molecular area, $A = 1/\Gamma$, can be determined. At low pressures (< 20 mN/m), a value ($A \sim 23$ Å^2/res) in good agreement with the interfacial area of β-sheet peptide models, is found [64]. At higher pressures, the interfacial area of CTX III falls to 5 Å^2/res, a low value as compared to the value found for the β-sheet peptide models (~ 15 Å^2/res). The transition between the two area values (5 and 23 Å^2/res) occurs in a very narrow range of surface pressures (between 20 and 30 mN/m). Considering that spectroscopic data have shown that the rigid structure of cardiotoxins does not change upon interaction with phospholipids [123], this behavior has been attributed to the capacity of cardiotoxins to be oriented 'flat' or 'edgewise' in the lipid film. According to Bougis et al. [124], the interaction between acidic phospholipids and cardiotoxins takes place in several steps: (1) an electrostatic interaction with the negatively charged polar heads of phospholipids; followed by (2) the penetration of at least the one hydrophobic loop of the cardiotoxin molecule; (3) the disorganization of the membrane; and, finally (4) a quick change of the bound cardiotoxin orientation. I would add that the orientation change of cardiotoxin from 'flat' to 'edgewise' may be the cause of the abrupt decrease in pressure observed in the course of the $\Delta\pi$–t experiments (Fig. 13).

5.5. *Penetration of nisin Z and other lantibiotic derivatives into phospholipid monolayers*

The lantibiotic nisin Z is used in the food industry as a preservative against Gram-positive bacteria [125]. Its activity was found to be influenced by the phospholipid composition of the target membrane [48] on the one hand and to be sensitive to structural changes in the first lanthionine ring [126] on the other hand. The monolayer penetration experiments show clearly that nisin Z interacts preferentially with acidic phospholipids and specially with cardiolipin and phosphatidylglycerol, the predominant lipids of Gram-positive bacteria [127,128]. The intercept of the $\Delta\pi - \pi_i$ plot with the $\Delta\pi$ axis is ~ 37 mN/m for

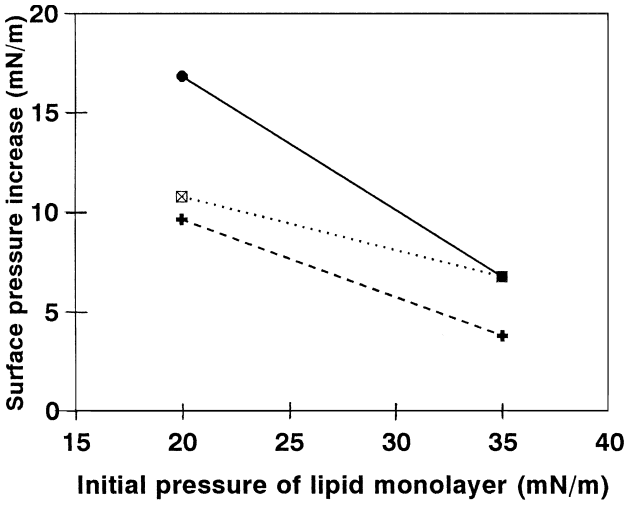

Fig. 14. Penetration of nisin Z and some of its mutants into DOPG monolayers. ●, Nisin Z; ⊠, [Gln7, Thr 18] nisin Z; +, [Dhb5] nisin Z. Peptide concentration: 1.8×10^{-5} M(res). Subphase: 10 mM Tris pH 7.4; Temperature not specified. Data from [127].

Escherichia coli cardiolipin monolayer and ~ 31 mN/m for DOPG monolayer, and although the authors gave no indication of the surface activity of nisin Z at a clean air/water interface, it can be asserted that nisin Z interacts specifically with both phospholipids. The fatty acyl chain composition has no influence on the penetration extent of nisin Z into phosphatidylglycerol monolayers. The affinity of nisin Z for zwitterionic phospholipids is much lower since the intercept with the $\Delta\pi$ axis is only 25 mN/m for DOPC and 16 mN/m for DOPE. Another lantibiotic, nisin A, containing a His instead of an Asn residue at position 27, with similar antimicrobial activities to nisin Z, exhibits the same penetration power into anionic phospholipid monolayers. On the contrary, changing dehydroalanine (Dha) at position 5 into dehydrobutyrine (Dhb) reduces the antibacterial activity 2–10-fold, and concurrently, as seen in Fig. 14, this mutant penetrates less extensively into acidic phospholipid monolayers. The same features are observed with the [Gln-17, Thr-18] mutant [126], which is less active than nisin Z against *Bacillus cereus* and *Streptococcus thermophilus*. Similarly, Breukink et al. [128] have shown that the less biologically active [Glu-32] mutant, obtained by introducing a negative charge in the cationic C-terminus of nisin Z (believed to initiate the nisin–membrane binding), inserted less

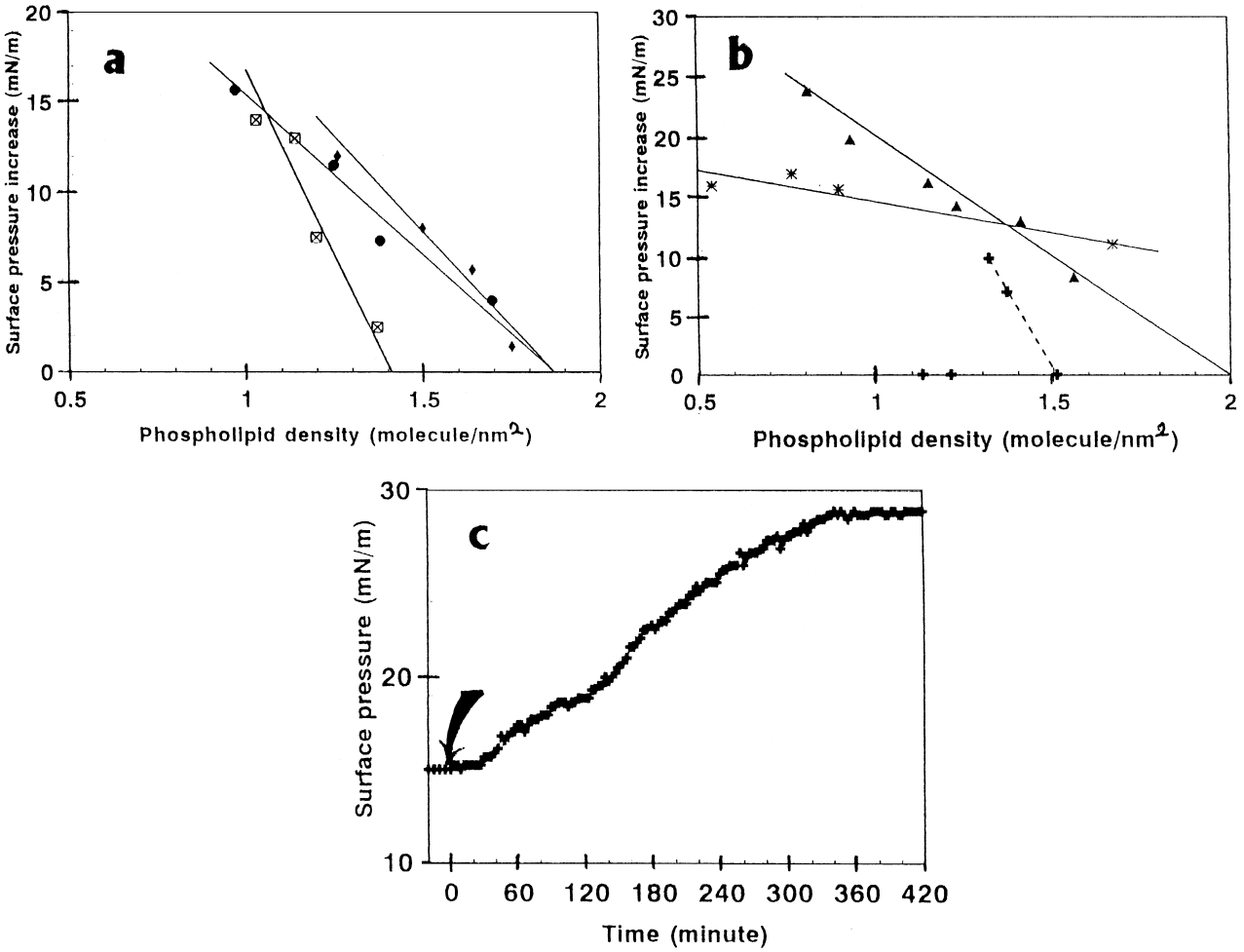

Fig. 15. Penetration of defensin A and androctonin into phospholipid monolayers. (a) Penetration of defensin A into phosphatidylcholine monolayers as a function of the initial density σ_i of the film. ● DMPC; ♦ DPPC; ⊠ egg lecithin [129]; (b) Penetration of: ——, defensin A [129] and - - -, androctonin (unpublished data) into anionic phospholipid monolayers. ▲, brain PS; ∗, cardiolipin; +, DMPG. (c) Time dependence of the androctonin penetration into a DMPG monolayer. Initial surface pressure of DMPG monolayer: 15 mN/m (unpublished data). Defensin A concentration: 4×10^{-6} M(res); androctonin concentration: 2.5×10^{-6} M(res). Subphase: 30 mM Tris-Cl pH 7.4 for defensin A, and 10 mM Tris-Cl, pH 7.4, 100 mM NaCl for androctonin. $T=20$°C.

efficiently than nisin Z into DOPG monolayers. Therefore, the lipid monolayer experiments appear to be a useful tool to establish a direct correlation between the antibacterial activity of the various nisins and their affinity for acidic phospholipids.

5.6. *Penetration of androctonin and defensin A [129] into phospholipid monolayers*

Androctonin is a constitutive peptide of scorpion hemolymph and defensin A an inducible one secreted in the insect hemolymph in response to bacterial injury [3]. Both are compact molecules (Fig. 4) possessing disulfide bridges and active against Gram-negative and Gram-positive bacteria. The activity of defensin A is known to be related to the formation of voltage-dependent channels [45], but the mode of action of androctonin is still under consideration. Hetru et al. [130] recently proposed a detergent-like mechanism (called the 'carpet-like' model [131]) of membrane disintegration. We have seen (Fig. 2a) that defensin A adsorbs very slowly at the air/water interface since no surface pressure increase was detectable in the first 70 min. On the contrary, defensin

A penetrates instantaneously into zwitterionic and acidic phospholipid monolayers. It can therefore be attested that defensin A interacts specifically with lipid membranes. The penetration extent of defensin A into the zwitterionic phosphatidylcholine monolayers is more sensitive to the lateral hindrance of the acyl chains than to their length, since the penetration profiles into DMPC and DPPC monolayers are very similar (Fig. 15a) with comparable exclusion densities ($\sigma_{ex} \sim 1.9$ molecule/nm^2), while the exclusion density in egg-PC monolayers is lower ($\sigma_{ex} \sim 1.4$ molecule/nm^2). Defensin A penetrates deeply into anionic phospholipid monolayers (Fig. 15b) as shown by comparing the behavior of defensin A into egg lecithin and bovine brain PS monolayers (both natural compounds with a mixture of unsaturated acyl chains). At a given $\sigma_i = 1.2$ molecule/nm^2, $\Delta\pi = 17$ mN/m into PS monolayers but only 9 mN/m into egg lecithin monolayers and concurrently the exclusion densities reach 2 and 1.4 lipid molecule/nm^2, respectively. In spite of the double charge of cardiolipin, the penetration of defensin A is less efficient into cardiolipin than into PS monolayers, and is not very dependent upon the lipid packing.

Androctonin penetrates very slightly into zwitterionic phospholipid monolayers: when the androctonin concentration in the subphase is 6.25×10^{-5} M(res), the surface pressure increase of the DMPC monolayer ($\sigma_i = 1.09$ DMPC molecule/nm^2) reaches only ~ 2 mN/m (a value near the $\Delta\pi_\infty^{AW}$ value as seen in Fig. 3), and androctonin no longer penetrates into the monolayer when σ_i rises to 1.38 DMPC molecule/nm^2. On the contrary, androctonin penetrates readily into the anionic DMPG monolayers. This is in good agreement with the recent findings of Hetru et al. [130] that fluorescent derivatives of androctonin bind only negatively charged phospholipid vesicles. The $\Delta\pi$–t plot (Fig. 15c) exhibits an inflection as though the penetration process occurs in two steps: (1) the first step corresponding to an accumulation of androctonin molecules under the DMPG monolayer, which may destabilize the lipid film but causes only a low pressure increase; and (2) the second one corresponding to the actual penetration of androctonin into the lipid monolayer. This hypothesis is corroborated by the analysis of the $\Delta\pi$–σ_i plot (Fig. 15b): a minimum lipid density (between 1.2 and 1.3 DMPG molecule/nm^2), equivalent to a minimum negative charge density, is needed for androctonin to penetrate the monolayer. Below this σ_i value, the highly hydrophilic androctonin must partitionate mainly in the subphase. This picture of the penetration events of androctonin into an anionic phospholipid monolayer agrees well with the 'carpet-like' model proposed for the mode of action of androctonin against bacterial cell membranes [130].

6. Mixed antimicrobial peptide/phospholipid monolayers

6.1. General considerations upon mixed (two-component) monolayers [54,132,133]

The usual procedure to obtain a two-component monolayer is to premix the two components in an appropriate spreading solvent and to spread the solution at the air/water interface. A number of monolayer properties derivable from surface pressure–area or surface potential-area isotherms are dependent upon monolayer composition. As in bulk liquid systems, the concept of 'ideality' plays a key role in the analysis of the mixed monolayer behavior: marked deviations from a linear relationship, and in particular the occurrence of a maximum or a minimum, indicate a significant deviation from ideality. These deviations are generally attributed to an *excess interaction* (i.e. specific interaction) between the monolayer components. The area of a two-component monolayer can be compared with that of the unmixed components at the same surface pressure, and, in the case of an ideal behavior:

$$A_{12} = X_1 A_1 + X_2 A_2 \quad (13)$$

where X is the molar fraction and the subscripts 1, 2 and 12 refer to the pure components 1 and 2 and to their mixtures, respectively.

Correspondingly, the surface potential should be given by:

$$\Delta V_{12} = X_1 \Delta V_1 + X_2 \Delta V_2 \quad (14)$$

If the components are immiscible (or ideally miscible), the area occupied by the mixed film will be the sum of the areas of the separate components, and reciprocally, any deviation of the A–X plot from ideality provides evidence for miscibility in the film.

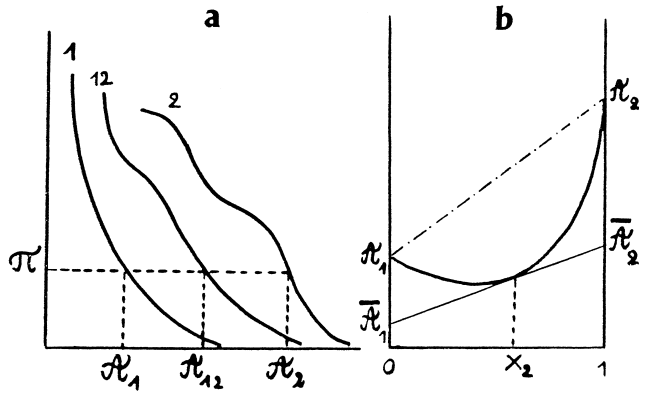

Fig. 16. Explanatory schema of mixed monolayer analysis. (a) Isotherm curves of the pure component monolayers, 1 and 2, and of a mixed monolayer, 12. (b) Area analysis as a function of the molar fraction, X_2, of component 2 in the mixed monolayer at a given surface pressure, π; -·-·-, additive rule drawn according to Eq. 13; ———, actual area values; determination of the partial areas $\mathcal{A}_1$ and $\mathcal{A}_2$ by the 'method of the tangents'.

Negative deviations from additive rules, such as Eqs. 13 and 14, generally indicate interactions between the film components. Positive deviations can be the sign of the formation of bidimensional clusters. However, these diagnoses must be corroborated by energy analysis as we will see latter. From the A–X plot it is also possible to determine graphically the partial molecular area of each component in the mixture by the classical 'method of the tangents': intercepts of the tangent to the A–X curve at a given X with the ordinate axis at $X_1 = 0$ and $X_1 = 1$ ($X_2 = 0$) give the partial molecular areas $\mathcal{A}_1$ and $\mathcal{A}_2$ in the mixture, of components 1 and 2, respectively (Fig. 16).

Another way to establish miscibility is the application, developed by Crisp, of the surface phase rule which is the derivation of the ordinary phase rule in bulk solution. If surface tension, temperature and external pressure are allowed to vary, the phase rule is written:

$$F = C^{B} + C^{S} - \Phi^{B} - \Phi^{S} + 3$$

where F is the number of degrees of freedom, C^{B} is the number of components in bulk equilibrated throughout the system, C^{S} is the number of components restricted to the surface, Φ^{B} is the number of bulk phases and Φ^{S} the number of monolayer phases in equilibrium with each other. $C^{B} = 2$ (air and water), $C^{S} = 2$ (components 1 and 2), $\Phi^{B} = 2$ (gaseous and liquid), therefore F becomes $5 - \Phi^{S}$, and, at constant temperature and external pressure:

$$F = 3 - \Phi^{S} \quad (15)$$

It should be noted that this criterion determines miscibility at a transition between two states, preferentially at collapse pressure (transition between condensed state and collapsed state), but also, by extension, at L-E–L-C transition because film collapse is not always easily measurable. If components 1 and 2 are miscible in all proportions, two homogeneous phases (either L-E and L-C or L-C and collapsed state) will be present in equilibrium with each other. Therefore $\Phi^{S} = 2$ and from Eq. 15 it can be deduced that the system possesses one degree of freedom ($F = 1$). Thus, a first order relation between the considered transition pressure and the composition of the film reveals a *complete miscibility* of the components. When a completely miscible monolayer exhibits no deviation from ideal behavior, the bidimensional analog of Raoult's law is obeyed. A *partial miscibility* is observed if, over a composition range, components 1 and 2 are immiscible. In this case three equilibrium surface phases will coexist and $F = 0$. Thus, in the range of immiscibility, π_t is invariant of the composition and the (π_t–X) curve must be flat over this region. In the case of *complete immiscibility*, the considered transition pressure will be independent of X.

Once it has been established that the components of the film are at least partially miscible, a more detailed examination of the thermodynamics of the system can provide further information on the energetics of the miscibility process and upon possible specific interactions between the two components. A method for determining the *excess free energy of mixing*, ΔG_m^{ex}, from the π–A isotherms of the mixed monolayers, has been developed by Goodrich:

$$\Delta G_m^{ex} = \int_{\pi^\circ}^{\pi} A_{12} d\pi - X_1 \int_{\pi^\circ}^{\pi} A_1 d\pi - X_2 \int_{\pi^\circ}^{\pi} A_2 d\pi \quad (16)$$

The lower limit of integration is often $\pi^\circ = 0$. The upper limit of integration may be arbitrarily selected. Negative values of ΔG_m^{ex} are the sign of strong interactions between the two components. A deep and steep minimum in the (ΔG_m^{ex}–X) plot at $X = x$ indicates the formation of a complex between the two components, the stoichiometry of which is x:1−x. Positive values of ΔG_m^{ex} reveal that mutual interac-

tions between the two components are weaker than interactions between the pure component molecules themselves: briefly, at least one component forms bidimensional aggregates. If $\Delta G_m^{ex} = 0$, the mixing is ideal.

6.2. Mixed gramicidin/lipid monolayers

From FTIR spectroscopy of mixed gramicidin A/DMPC monolayers, Ulrich and Vogel [134] reported that the structure of gramicidin A in the lipid monolayer could be assigned to a $\beta^{6.3}$ helix thought to be the conformation which, by N–N dimerization, forms the functional channel [135]. They stated also that, as seen above for pure gramicidin A monolayers [89,90], the orientation of the helix in mixed gramicidin A/DMPC monolayers is markedly dependent on the applied surface pressure: at low pressure, the helix lay flat on the surface, whereas at high pressures, the helix is oriented vertically. Van Mau et al. [136] and Tournois et al. [90] have studied the peptide–lipid interactions in mixed gramicidin A/phospholipid monolayers. The former reported no deviations from ideality in the area–composition diagram of the mixed GA/DOPC monolayers and the inflection in the isotherm occurs at the same pressure ($\sim$13 mN/m) on the range of composition where it is detectable ($0.5 \leq X_{GA} \leq 1$). Furthermore, the presence of DOPC in the monolayer has no effect on the surface potential. These features indicate a complete immiscibility of gramicidin A and DOPC. Although Tournois et al. [90] observed negative variations (about -5% at 5 mN/m and -10% at 30 mN/m) in the A–X plot of GA/DOPC monolayers, the inflection pressure being invariant, the contraction of the monolayer can be attributed to a space-filling mechanism [132], and a complete immiscibility of gramicidin A and DOPC in mixed monolayers can also be deduced. Gramicidin A, as well as its analogs, were also found to be immiscible with glyceromonooleate, a lipid currently used in single-channel experiments [137,138]. Therefore, it seems well established that, in the prevailing conditions of the mixed GA/lipid monolayer experiments, gramicidin A is not miscible with the lipid phase. This is a questionable conclusion, considering the known membrane channel activity of gramicidin A. I wish to put forward a tentative explanation. People working on single-channel experiments know that traces of gramicidin A are enough to set off the conducting activity and that, even at low concentration, the very hydrophobic gramicidin A aggregates. In spite of that, in mixed monolayer experiments, the smallest molar fraction considered was 10%, i.e. 62.5% of peptide residues with regards to lipid molecules. It is probable that working at 100-fold lower gramicidin A concentrations would give different results. Shapovalov et al. [139] have just supported this opinion: after addition of gramicidin A to the subphase, at concentrations ranging between 1 and 5×10^{-6} M(res), they observed a shift of the π–A isotherms of DPPC monolayers and a considerable reduction of their surface potential. Furthermore, Wallace and Janes [140] have shown that gramicidin A co-crystallizes with DPPC giving an additional proof of their miscibility.

6.3. Mixed melittin/lipid monolayers

Fidelio et al. [103] have studied the behavior of melittin in mixed monolayers with several types of lipids. As shown in Fig. 17a, the A–X_{mel} plot of melittin/DMPC monolayers exhibits negative deviations at a low melittin molar fraction ($X_{mel} \leq 0.04$). Up to this molar fraction, the area–composition plot follows the additivity rule and concurrently, the isotherms exhibit two collapse pressures, indicative of a phase separation in the film. The mixed film is more stable than pure DMPC monolayer as proved by its higher collapse pressure. All these features suggest the formation of a melittin–DMPC complex with a 1:24 stoichiometry. From gel filtration and light scattering of lipid vesicles, Dufourcq et al. [141] found a stoichiometry of the same magnitude order for melittin–DPPC complexes (one melittin for 25 ± 7 DPPC). The application of the phase rule to the collapse pressure–composition diagram can give further information, which is set down in the legend of Fig. 17b.

Fidelio et al. [103] also studied the interactions of melittin with the negatively charged ganglioside GM1. The A–X_{mel} plot of melittin/GM1 monolayers presents negative deviations over the whole range of composition, indicating strong interactions between the two components. The maximum deviation in the area–composition plot occurs around $X_{mel} = 0.25$, suggesting the formation of a 1:3 melit-

tin–GM_1 complex. The collapse pressure–composition diagram indicates that a phase separation occurs up to $X_{mel} = 0.5$. This result can be correlated with the finding that melittin induces a ratio-dependent phase change from bilayer structure to hexagonal H_{II} phase in melittin–cardiolipin systems [142].

6.4. Mixed bombolitin III/phospholipid monolayers

Another way to obtain mixed monolayers is to spread the lipid film onto a peptide solution. This was the choice of Signor et al. [100] when studying the interaction of bombolitin III with phospholipid monolayers. It is clear that this method does not allow a precise control of the peptide amount present at the interface. However, as argued by the authors, the system reaches an equilibrium corresponding to the peptide amount adsorbed by the monolayer as a function of the peptide concentration in the subphase. Besides, this procedure is more representative of the natural association process of a soluble peptide with a biological membrane. From these experiments it appears that there is a rapid adsorption of bombolitin III into phospholipid monolayers in conditions (low ionic strength and acidic pH) where the peptide does not adsorb at a clean air/water interface. This adsorption is clearly demonstrated by the expansion of the phospholipid monolayer over time. Upon compression, the mixed bombolitin III/DPPC monolayers display a two-phase behavior, whereas the bombolitin III/DMPC monolayers display a one-phase behavior. Introducing traces of a fluorescent lipid probe into the phospholipid phase allows the observation of the mixed monolayer by means of an epifluorescence microscope. In this way, the formation of phase-separated domains of bombolitin III in the DPPC monolayer can be visualized.

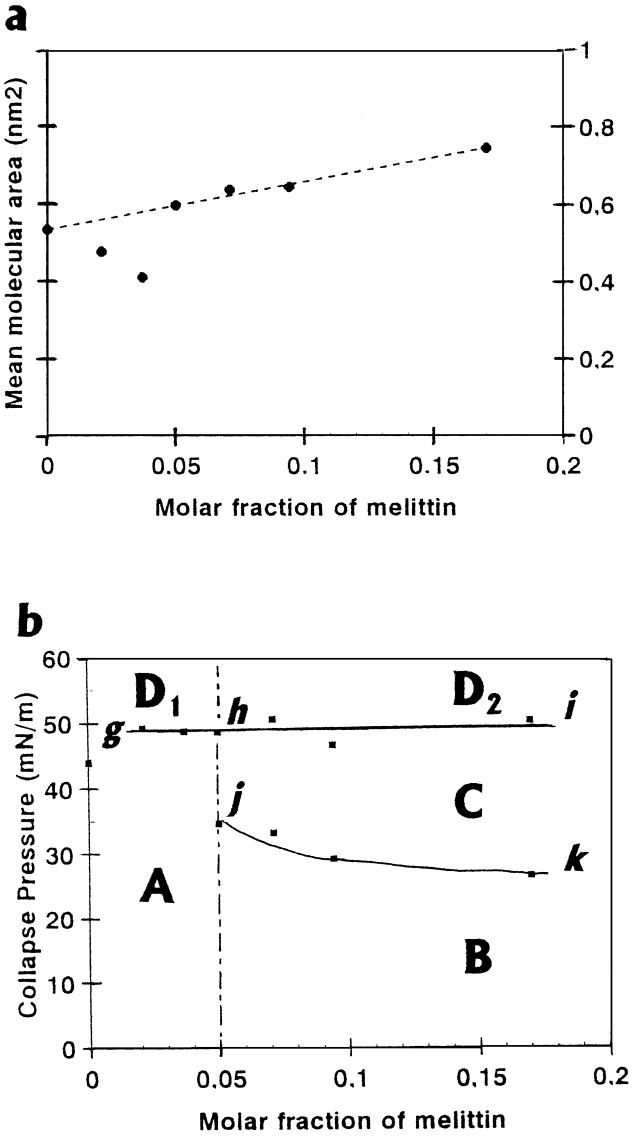

→

Fig. 17. Mixed melittin/DMPC monolayers. (a) Area–composition diagram. The area taken into consideration is A_s (see Fig. 5b); - - -, additive rule drawn according to Eq. 13. (b) Collapse pressure–composition diagram. Analysis of the π_c–X_{mel} diagram according to Eq. 15: the line *ghi* corresponds to the collapse pressure of the 1:24 melittin–DMPC complex; three phases are in equilibrium along the line *gh* (since $F = 0$): excess DMPC and the melittin–DMPC complex miscible in a liquid state, excess DMPC in the collapsed state and the melittin–DMPC complex in the collapsed state; in the same way, three phases are in equilibrium along the line *hi*: the melittin–DMPC complex in a liquid state, excess melittin in the collapsed state and the melittin–DMPC complex in the collapsed state; two phases are in equilibrium along the line *jk* (since $F = 1$): excess melittin and the melittin–DMPC complex miscible in a liquid state and melittin in the collapsed state; then, the π_c–X_{mel} diagram can be divided into several regions: in region A, the melittin–DMPC complex and the excess DMPC are both in a liquid state and miscible. In region B, the complex and the excess melittin are miscible in a liquid state. In region C, melittin is in a collapsed state immiscible with the complex in a liquid state. In region D_1, excess DMPC and the complex are both in the collapsed state and immiscible and in region D_2, excess melittin and the complex are both in a collapsed state and immiscible. Data from [103].

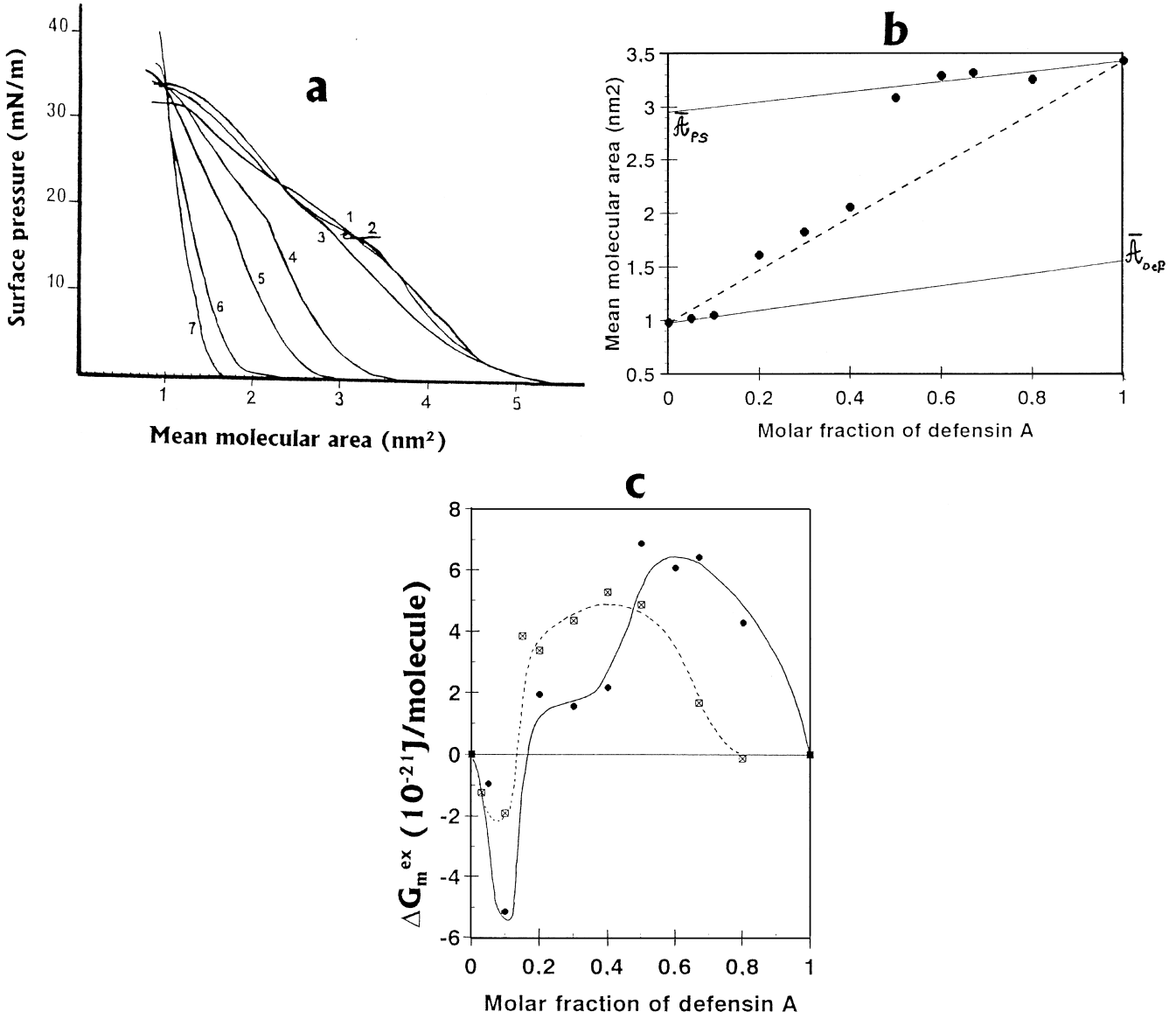

Fig. 18. Mixed defensin A/phospholipid monolayers. (a) Compression isotherms of mixed defensin A/PS monolayers. Curve 1, $X_{def} = 1$ (pure defensin A monolayer); curve 2, $X_{def} = 0.8$; curve 3, $X_{def} = 0.5$; curve 4, $X_{def} = 0.4$; curve 5, $X_{def} = 0.2$; curve 6, $X_{def} = 0.1$; curve 7, $X_{def} = 0$ (pure PS monolayer) [129]. (b) Mean molecular area of mixed defensin A/PS monolayers at 15 mN/m; - - -, additive rule drawn according to Eq. 13; data from [129]. (c) Thermodynamics of the mixing process of defensin A and phospholipids in mixed monolayers. Excess free energy of mixing (calculated according to Eq. 16) as a function of composition. Upper limit of integration: 20 mN/m. Subphase: 30 mM Tris-Cl pH 7.4. $T = 20$°C. ●, bovine brain PS; ⊠, egg lecithin (unpublished data).

6.5. *Mixed defensin A/phospholipid monolayers [129]*

The defensin A behavior in mixed films has been studied with two natural phospholipids, egg lecithin and bovine brain PS. From the analysis of the π–A curves of the mixed defensin A–phospholipid monolayers, the formation of a defensin A–phospholipid complex was suggested with both phospholipids. The defensin A–PS monolayers (Fig. 18a) are more stable than a pure defensin A monolayer, as attested by their higher collapse pressures ($\pi_c \sim 36$ mN/m for the defensin A–PS complex instead of ~ 31 mN/m for the pure defensin A). The area–composition diagram (Fig. 18b) shows negative deviations from ideality in the $0 < X_{def} < 0.2$ range, indicating excess interactions between defensin A and PS. However,

large positive deviations in the defensin-rich region ($X_{def} \geq 0.5$) suggest that the defensin A–PS complexes form clusters in the defensin A monolayers. In this region, the partial molecular area of PS is roughly the same as the area of defensin A, indicating that in the complex, the PS molecules are intimately bound to defensin A and occupy the same surface. In order to determine precisely the stoichiometry of the defensin A–phospholipid complexes, we calculated the excess energy of mixing ΔG_m^{ex} according to Eq. 16. The results are shown in Fig. 18c. The ΔG_m^{ex}–composition plot presents a deep and narrow minimum at the same $X_{def} \sim 0.1$ in both cases (egg lecithin and PS), indicating the formation of 1:9 defensin A–phospholipid complexes. However, the defensin A–PS complex is energetically more stable than the complex with lecithin since $\Delta G_m^{ex} \sim -5 \times 10^{-21}$ J/molecule for the defensin A–PS complex instead of -2×10^{-21} J/molecule in the case of the defensin A–lecithin complex. In the $0.2 \leq X_{def} < 1$ range, the excess energy of mixing presents positive values, indicating the formation of bidimensional aggregates either of the defensin A–phospholipid complex or of defensin A itself. In the case of defensin A/PS monolayers, the (ΔG_m^{ex}–X_{def}) plot presents a plateau at 2×10^{-21} J/molecule before reaching high energy values, suggesting that there may be two steps in the aggregation process.

It should be noted that: (1) the peptide rich-region of the composition diagrams is generally devoid of interest since the aim of the study was the determination of the peptide behavior *in* lipid membranes. It is obvious in this study that it would have been preferable to obtain more values in the $0 < X_{def} < 0.2$ range. As a matter of fact, the small number of values in the lipid-rich region leads to an uncertainty on the complex stoichiometry which actually varies between 1:9 and 1:4; (2) on the basis of area–composition and transition pressure–composition diagrams only, we previously concluded that the defensin A–phospholipid complexes have a 1:4 stoichiometry. The energy analysis presented here suggests that the actual value is nearer 1:9 than 1:4. This last result agrees well with the findings of D. Sy (personal communication) deduced from investigation of the electrostatic potential surfaces of defensin A. As a matter of fact, one of the molecular faces is markedly more electropositive than the others with its side chains directed outwards. This positive face contains not only the β-sheet Arg-26, Arg-39 and Lys-33 cationic residues as well as the hydrophilic residues Asn-31 and Asn-40, but also the His-19 and Arg-23 residues belonging to the α-helix. Therefore, seven anionic lipids at least could interact strongly with this particular face of defensin A.

7. Conclusion

The monolayer technique has proved to be an invaluable approach for the study of the physicochemical properties of peptides at hydrophilic/hydrophobic interfaces. Moreover, the lipid monolayer provides a unique model membrane of great interest and reliability in understanding the insertion mechanism of antimicrobial peptides into cell membranes. We have restricted this review to the basic Langmuir film balance experiments, but it should be pointed out that numerous complementary techniques have been developed with the aim of improving and extending the monolayer technique possibilities. Thus, various spectroscopic methods allow direct observation of the phase behavior of the peptide or lipid monolayer during compression: among them, epifluorescence microscopy [100,143] and Brewster angle microscopy [143] are the most currently employed. Similarly, in situ infrared spectroscopy allows the determination of the structure and orientation of the peptide at the interface [134,144]. The Langmuir–Blodgett technique [145] has long been used to transfer monolayers onto solid supports. Transferred monolayers can be studied by spectroscopic methods such as CD [146–148], IR [120,147,148], X-ray diffraction [149] or atomic force microscopy [150]. This list is not exhaustive, but is given only to point out the wide range of technologies developed around the monolayer technique and another review could be devoted to such a subject.

Acknowledgements

I wish to thank Denise Sy for her valuable help in the PDB structure search and representation. Our fruitful discussions on androctonin and defensin A behavior were always greatly appreciated.

References

[1] C.L. Bevins, M. Zasloff, Annu. Rev. Biochem. 59 (1990) 395–414.
[2] C.E. Dempsey, Biochim. Biophys. Acta 1041 (1990) 143–161.
[3] J.A. Hoffmann, Ch. Hetru, Immunol. Today 13 (1992) 411–415.
[4] I. Cornut, E. Thiaudière, J. Dufourcq, in: R.M. Epand (Ed.), The Amphipathic Helix, CRC Press, 1993, pp. 173–219.
[5] S. Cociancich, P. Bulet, Ch. Hetru, J.A. Hoffmann, Parasitol. Today 10 (1994) 132–139.
[6] A.G. Rao, Mol. Plant-Microbe Interact. 8 (1995) 6–13.
[7] H.G. Boman, Annu. Rev. Immunol. 13 (1995) 61–92.
[8] W.L. Maloy, U.P. Kari, Biopolymers 37 (1995) 105–122.
[9] H.-G. Sahl, R.W. Jack, G. Bierbaum, Eur. J. Biochem. 230 (1995) 827–853.
[10] S.H. White, W.C. Winley, M.E. Selsted, Curr. Opin. Struct. Biol. 5 (1995) 521–527.
[11] R.I. Lehrer, T. Ganz, Ann. New York Acad. Sci. 797 (1996) 228–239.
[12] R.E.W. Hancock, Lancet 349 (1997) 418–422.
[13] B. Bechinger, J. Membr. Biol. 156 (1997) 197–211.
[14] W.F. Broekaert, B.P. Cammue, M.F. De Bolle, K. Thevissen, G.W. De Samblanx, R.W. Osborn, Crit. Rev. Plant Sci. 16 (1997) 297–323.
[15] P.M. Hwang, H.J. Vogel, Biochem. Cell Biol. 76 (1998) 235–246.
[16] R.E.W. Hancock, R. Lehrer, Trends Biotechnol. 16 (1998) 82–87.
[17] K. Matsuzaki, Biochim. Biophys. Acta 1376 (1998) 391–400.
[18] J.M. Schröder, Biochem. Pharmacol. 57 (1999) 121–134.
[19] A.W. Bernheimer, Biochim. Biophys. Acta 344 (1974) 27–50.
[20] E. Katz, A.L. Demain, Bacteriol. Rev. 41 (1977) 449–474.
[21] L. Ehret-Sabatier, D. Loew, M. Goyffon, P. Fehlbaum, J.A. Hoffmann, A. van Dorsselaer, Ph. Bulet, J. Biol. Chem. 271 (1996) 29537–29544.
[22] J. Lambert, E. Keppi, J.L. Dimarcq, C. Wicker, J.M. Reichhart, B. Dunbar, P. Lepage, A. van Dorsselaer, J. Hoffmann, J. Fothergill, D. Hoffmann, Proc. Natl. Acad. Sci. USA 86 (1989) 262–266.
[23] B. Cornet, J.-M. Bonmatin, Ch. Hetru, J.A. Hoffmann, M. Ptak, F. Vovelle, Structure 3 (1995) 435–448.
[24] M. Zasloff, B. Martin, H.C. Chen, Proc. Natl. Acad. Sci. USA 85 (1988) 910–913.
[25] P. Eisenhauer, S. Harwig, R. Lehrer, Infect. Immunol. 60 (1992) 3556–3565.
[26] E. Habermann, J. Jentsch, Hoppe-Seyler's Z Physiol. Chem. 348 (1967) 37–50.
[27] A. Argolias, J. Pisano, J. Biol. Chem. 260 (1985) 1437–1444.
[28] A.I. Louw, Biochim. Biophys. Acta 336 (1974) 470–480.
[29] E. Gross, J.L. Morrell, J. Am. Chem. Soc. 93 (1970) 4634–4635.
[30] G. Buchman, S. Banerjee, J. Hansen, J. Biol. Chem. 263 (1988) 16260–16266.
[31] J. Fitton, A. Dell, W. Shaw, FEBS Lett. 115 (1980) 209–212.
[32] R. Sarges, B. Witkop, J. Am. Chem. Soc. 87 (1965) 2011–2020.
[33] E. Katz, A.L. Demain, Bacteriol. Rev. 41 (1977) 449–474.
[34] J.F. Faucon, J. Dufourcq, C. Lussan, FEBS Lett. 102 (1979) 187–190.
[35] M. Jackson, H. Mantsch, J. Spencer, Biochemistry 31 (1992) 7289–7293.
[36] R. Urrutia, R.A. Cruciani, J.L. Barker, B. Kachar, FEBS Lett. 247 (1988) 17–21.
[37] J.E. Fitton, FEBS Lett. 102 (1981) 257–260.
[38] E. Thiaudière, O. Siffert, J.-C. Talbot, J. Bolard, J.E. Alouf, J. Dufourcq, Eur. J. Biochem. 195 (1991) 203–213.
[39] E. Bairaktari, D.F. Mierke, S. Mammi, E. Peggion, Biochemistry 29 (1990) 10097–10102.
[40] R. Maget-Dana, J.-M. Bonmatin, Ch. Hetru, M. Ptak, J.-C. Maurizot, Biochimie 77 (1995) 240–244.
[41] H. Nikaido, in: Membrane Transport and Information Storage, Alan R. Liss, 1990, pp. 165–190.
[42] K. Matsuzaki, K.I. Sugishita, N. Fujii, K. Miyajima, Biochemistry 34 (1995) 3423–3429.
[43] K.L. Piers, M.H. Brown, R.E.W. Hancock, Antimicrob. Agents Chemother. 38 (1994) 2311.
[44] B.L. Kagan, M.E. Selsted, T. Ganz, R.I. Lehrer, Proc. Natl. Acad. Sci. USA 87 (1990) 210–214.
[45] S. Cociancich, A. Ghazi, Ch. Hetru, J.A. Hoffmann, L. Letellier, J. Biol. Chem. 268 (1993) 19239–19245.
[46] H. Duclohier, G. Molle, G. Spach, Biophys. J. 56 (1989) 1017–1021.
[47] M.T. Tosteson, D.C. Tosteson, Biophys. J. 36 (1981) 109–116.
[48] M.J. Garcia Garcera, M.G. Elferink, A.J. Driessen, W.N. Konings, Eur. J. Biochem. 212 (1993) 417–428.
[49] C.P. Hill, J. Yee, M.E. Selsted, D. Eisenberg, Science 251 (1991) 1481–1485.
[50] D.W. Urry, Proc. Natl. Acad. Sci. USA 68 (1972) 672–676.
[51] G. Spach, H. Duclohier, G. Molle, J.-M. Valleton, Biochimie 71 (1989) 11–21.
[52] W.L. Duax, J.F. Griffin, D.A. Langs, G.D. Smith, P. Grochulski, V. Pletnev, V. Ivanov, Biopolymers 40 (1996) 141–155.
[53] A.W. Adamson, Physical Chemistry of Surfaces, 3rd edn., J. Wiley and Sons, New York, 1976.
[54] G.L. Gaines, Insoluble Monolayers at Liquid–Gas Interfaces, Prigogine (Ed.), J. Wiley and Sons, New York, 1966.
[55] J.W. McBain, R.C. Bacon, H.D. Bruce, J. Chem. Phys. 7 (1939) 818–821.
[56] J.W. Gibbs, Collected Works, Vol. 1, Longmans, New York, 1931.
[57] R. Bresow, T. Guo, Proc. Natl. Acad. Sci. USA 87 (1990) 167–169.
[58] R. Pethig, Dielectric and Electronic Properties of Biological Materials, Wiley, New York, 1979.
[59] K. Birdi, V. Gevod, O. Ksenzhek, E. Stenby, K. Rasmussen, Colloid Polymer Sci. 261 (1983) 767–775.
[60] N. Lakhsminarayanaiah, Equations of Membrane Biophysics, Academic Press, London, 1984.

[61] R. Miller, G. Kretzschmar, Adv. Colloid Interface Sci. 37 (1991) 97–121.
[62] F. MacRichtie, Colloids Surfaces A. Physicochem. Eng. Aspects 76 (1993) 159–166.
[63] A.F. Ward, L. Tordai, J. Chem. Phys. 14 (1946) 453–461.
[64] R. Maget-Dana, D. Lelièvre, A. Brack, Biopolymers 49 (1999) 415–423.
[65] D.E. Graham, M.C. Phillips, J. Colloid Interface Sci. 70 (1979) 403–414.
[66] R. Maget-Dana, M. Ptak, Colloids Surfaces B: Biointerfaces 7 (1996) 135–143.
[67] P. Suttiprasit, V. Krisdhasima, J. McGuire, J. Colloid Interface Sci. 154 (1992) 316–326.
[68] P. Bougis, H. Rochat, G. Piéroni, R. Verger, Biochemistry 20 (1981) 4915–4920.
[69] O.S. Ksenzhek, V.S. Gevod, A.M. Omel'chenko, S.N. Semenov, A.I. Sotnichenko, Mol. Biol. (Mosk.) 12 (1978) 1057–1065.
[70] E. Schröder, K. Lübke, M. Lehmann, I. Beetz, Experientia 27 (1971) 764–765.
[71] A.S. Tatham, R.C. Hider, A.F. Drake, Biochem. J. 211 (1983) 683–686.
[72] T.C. Terwilliger, L. Weissman, D. Eisenberg, Biochim. Biophys. Acta 37 (1982) 353–361.
[73] G.D. Fidelio, B. Maggio, F.A. Cumar, Biochem. J. 203 (1982) 717–725.
[74] M.J. Dufton, R.C. Hider, Pharmacol. Ther. 36 (1988) 1–40.
[75] W. Jahnke, D.F. Mierke, L. Beress, H. Kessler, J. Mol. Biol. 240 (1994) 445–458.
[76] N. Mandard, D. Sy, C. Maufrais, J.-M. Bonmatin, Ph. Bulet, Ch. Hetru, F. Vovelle, J. Biomol. Struct. Dynam. 17 (1999) 367–380.
[77] F. Uraizee, G. Narsimhan, J. Colloid Interface Sci. 146 (1991) 169–178.
[78] R. Maget-Dana, A. Brack, D. Lelièvre, Supramol. Sci. 4 (1997) 365–368.
[79] R. Maget-Dana, Ch. Hetru, M. Ptak, Thin Solid Films 284/285 (1996) 841–844.
[80] G. Colacicco, M.K. Basu, A.R. Buchelew, A.W. Bernheimer, Biochim. Biophys. Acta 465 (1977) 378–390.
[81] C.W. Cumper, A.E. Alexander, Trans. Faraday Soc. 46 (1950) 235–238.
[82] M. Bhakoo, T.H. Birbeck, J.H. Freer, Biochemistry 21 (1982) 6879–6883.
[83] G. Schwarz, S. Taylor, Langmuir 11 (1995) 4341–4346.
[84] K.S. Birdi, Lipid and Biopolymer Monolayers at Liquid Interfaces, Plenum Press, New York, 1989.
[85] J.W. Taylor, Biochemistry 29 (1990) 5364–5373.
[86] K. Kobayashi, J.R. Granja, M.R. Ghadiri, Angew. Chem. Int. Ed. Engl. 34 (1995) 95–98.
[87] K. Birdi, J. Colloid Interface Sci. 43 (1973) 545–547.
[88] G. Kemp, K.A. Jacobson, C.E. Wenner, Biochim. Biophys. Acta 255 (1972) 493–501.
[89] N. Davion-Van Mau, P. Daumas, D. Lelièvre, Y. Trudelle, F. Heitz, Biophys. J. 51 (1987) 843–845.
[90] H. Tournois, P. Gieles, R. Demel, J. de Gier, B. de Kruijff, Biophys. J. 55 (1989) 557–569.
[91] H.E. Ries, H. Swift, Colloids Surfaces 40 (1989) 145–165.
[92] P. Lavigne, P. Tancrède, F. Lamarche, J.-J. Max, Langmuir 8 (1992) 1988–1993.
[93] W. Veatch, E. Fossel, E. Blout, Biochemistry 13 (1974) 5249–5256.
[94] R. Brasseur, J.A. Killian, B. de Kruijff, J.M. Ruysschaert, Biochim. Biophys. Acta 903 (1987) 11–17.
[95] B.R. Malcolm, Prog. Surf. Membr. Sci. 7 (1973) 183–229.
[96] T. Vogt, J. Killian, R. Demel, B. De Kruijff, Biochim. Biophys. Acta 1069 (1991) 157–164.
[97] D. Jones, E. Hayon, D. Busath, Biochim. Biophys. Acta 861 (1986) 62–67.
[98] W.F. DeGrado, F.J. Kézdy, E.T. Kaiser, J. Am. Chem. Soc. 103 (1981) 679–681.
[99] G. Sessa, J.H. Freer, G. Colacicco, G. Weissmann, J. Biol. Chem. 244 (1969) 3575–3582.
[100] G. Signor, S. Mammi, E. Peggion, H. Ringsdorf, A. Wagenknecht, Biochemistry 33 (1994) 6659–6670.
[101] G. Wackerbauer, I. Weis, G. Schwarz, Biophys. J. 71 (1996) 1422–1427.
[102] V. Gevod, K. Birdi, Biophys. J. 45 (1984) 1079–1083.
[103] G.D. Fidelio, B. Maggio, F.A. Cumar, Biochim. Biophys. Acta 862 (1986) 49–56.
[104] V. Gevod, K. Birdi, Colloid Polymer Sci. 265 (1987) 257–261.
[105] H.T. Tien, Bilayer Lipid Membranes (BLM): Theory and Practice, M. Dekker, 1974.
[106] G.D. Eytan, Biochim. Biophys. Acta 694 (1982) 185–202.
[107] R.A. Demel, Subcell. Biochem. 23 (1994) 83–120.
[108] H. Brockman, Curr. Opin. Struct. Biol. 9 (1999) 438–443.
[109] D. Marsh, Biochim. Biophys. Acta 1286 (1996) 183–223.
[110] S. Feng, Langmuir 15 (1999) 998–1010.
[111] B. Pethica, Trans Faraday Soc. 51 (1955) 1402–1411.
[112] H.S. Hendrickson, P. Fan, D. Kaufman, D. Kleiner, Arch. Biochem. Biophys. 227 (1983) 242–247.
[113] C.R. Flach, F.G. Prendergast, R. Mendelsohn, Biophys. J. 70 (1996) 539–546.
[114] S. Ohki, E. Marcus, D.K. Sukumaran, K. Arnold, Biochim. Biophys. Acta 1194 (1994) 223–232.
[115] A.F. Mingotaud, C. Mingotaud, L.K. Patterson, in: Handbook of Monolayers, Academic Press, New York, 1993, pp. 778–986.
[116] B. Stanislawski, H. Rüterjans, Eur. Biophys. J. 15 (1987) 1–12.
[117] G. Schwarz, G. Beschiaschvili, Biochim. Biophys. Acta 979 (1989) 82–90.
[118] Y. Ebara, Y. Okahata, Langmuir 9 (1993) 574–576.
[119] J. Bello, H.R. Bello, E. Granados, Biochemistry 21 (1982) 461–465.
[120] S.-F. Sui, H. Wu, Y. Guo, K.-S. Chen, J. Biochem. 116 (1994) 482–487.
[121] C. Altenbach, W. Froncisz, J. Hyde, W. Hubbel, Biophys. J. 56 (1989) 1183–1191.

[122] C. Dempley, G. Butler, Biochemistry 31 (1992) 11973–11977.
[123] M. Pezolet, L. Duchesneau, P. Bougis, J.F. Faucon, J. Dufourcq, Biochim. Biophys. Acta 704 (1982) 515–523.
[124] P. Bougis, M. Tessier, J. Van Rietschoten, H. Rochat, J.F. Faucon, J. Dufourq, Mol. Cell. Biochem. 55 (1983) 49–64.
[125] J. Delves-Broughton, J. Soc. Dairy Technol. 43 (1990) 73–76.
[126] O. Kuipers, H. Rollema, W. Yap, H. Boot, R. Siezen, W. De Vos, J. Biol. Chem. 267 (1992) 24340–24346.
[127] A.R. Demel, T. Peelen, R. Siezen, B. De Kruijff, O. Kuipers, Eur. J. Biochem. 235 (1996) 267–274.
[128] E. Breukink, C. van Kraaij, R. Demel, R. Siezen, O. Kuipers, B. de Kruijff, Biochemistry 36 (1997) 6968–6976.
[129] R. Maget-Dana, M. Ptak, Biophys. J. 73 (1997) 2527–2533.
[130] Ch. Hetru, L. Letellier, Z. Oren, J.A. Hoffmann, Y. Shai, Biochem. J., in press.
[131] E. Gazit, A. Boman, H. Boman, Y. Shai, Biochemistry 34 (1995) 11470–11488.
[132] I. Costin, G. Barnes, J. Colloid Interface Sci. 51 (1975) 106–121.
[133] K. Bacon, G. Barnes, J. Colloid Interface Sci. 67 (1978) 70–77.
[134] W.P. Ulrich, H. Vogel, Biophys. J. 76 (1999) 1639–1647.
[135] B.A. Wallace, Biophys. J. 49 (1986) 295–306.
[136] N. Van Mau, Y. Trudelle, P. Daumas, F. Heitz, Biophys. J. 54 (1988) 563–567.
[137] A. Benayad, D. Benamar, N. Van Mau, G. Page, F. Heitz, Eur. Biophys. J. 20 (1991) 209–213.
[138] N. Van Mau, B. Bonnet, A. Benayad, F. Heitz, Eur. Biophys. J. 22 (1994) 447–452.
[139] V.L. Shapovalov, E.A. Kotova, T.I. Rokitskaya, Y.N. Antonenko, Biophys. J. 77 (1999) 299–305.
[140] B.A. Wallace, R.W. Janes, J. Mol. Biol. 217 (1991) 625–627.
[141] J. Dufourcq, J.F. Faucon, G. Fourche, J.J. Dasseux, M. Le Maire, T. Gulik-Krzywicki, Biochim. Biophys. Acta 859 (1986) 33–46.
[142] A.M. Batenburg, J.C. Hibbeln, A.J. Verkleij, B. de Kruijff, Biochim. Biophys. Acta 903 (1987) 142–154.
[143] M. Lipp, K.Y.C. Lee, A. Waring, J.A. Zsadzinski, Biophys. J. 72 (1997) 2783–2804.
[144] S. Castano, B. Desbat, M. Laguerre, J. Dufourq, Biochim. Biophys. Acta 1416 (1999) 176–194.
[145] G.G. Roberts, Langmuir–Blodgett Films, Plenum, New-York, 1990.
[146] D.G. Cornell, J. Colloid Interface Sci. 70 (1979) 167–180.
[147] R. Maget-Dana, G. Bolbach, Y. Trudelle, Biopolymers 35 (1994) 629–637.
[148] M. Boncheva, H. Vogel, Biophys. J. 73 (1997) 1056–1072.
[149] S. Ludtke, K. He, H. Huang, Biochemistry 34 (1995) 16764–16769.
[150] N. Van Mau, V. Vié, L. Chaloin, E. Lesniewska, F. Heitz, C. Le Grimellec, J. Membr. Biol. 167 (1999) 241–249.